Low Forces Push the Maturation of Neural Precursors into Neurons

Sara De Vincentiis,* Matteo Baggiani, Francesca Merighi, Valentina Cappello, Jakub Lopane, Mariachiara Di Caprio, Mario Costa, Marco Mainardi, Marco Onorati, and Vittoria Raffa*

Mechanical stimulation modulates neural development and neuronal activity. In a previous study, magnetic "nano-pulling" is proposed as a tool to generate active forces. By loading neural cells with magnetic nanoparticles (MNPs), a precise force vector is remotely generated through static magnetic fields. In the present study, human neural stem cells (NSCs) are subjected to a standard differentiation protocol, in the presence or absence of nano-pulling. Under mechanical stimulation, an increase in the length of the neural processes which showed an enrichment in microtubules, endoplasmic reticulum, and mitochondria is found. A stimulation lasting up to 82 days induces a strong remodeling at the level of synapse density and a re-organization of the neuronal network, halving the time required for the maturation of neural precursors into neurons. The MNP-loaded NSCs are then transplanted into mouse spinal cord organotypic slices, demonstrating that nano-pulling stimulates the elongation of the NSC processes and modulates their orientation even in an ex vivo model. Thus, it is shown that active mechanical stimuli can guide the outgrowth of NSCs transplanted into the spinal cord tissue. The findings suggest that mechanical forces play an important role in neuronal maturation which could be applied in regenerative medicine.

S. De Vincentiis, M. Baggiani, F. Merighi, J. Lopane, M. Onorati, V. Raffa
Department of Biology
Università di Pisa
Pisa 56127, Italy
E-mail: sara.devincentiis@biologia.unipi.it; vittoria.raffa@unipi.it
V. Cappello
Center for Materials Interfaces
Istituto Italiano di Tecnologia
Pontedera 56025, Italy
M. Di Caprio
Laboratory of Biology "Bio@SNS"
Scuola Normale Superiore
Piazza dei Cavalieri 7, Pisa 56126, Italy
M. Costa, M. Mainardi
Neuroscience Institute
National Research Council
via Giuseppe Moruzzi 1, Pisa 56124, Italy

1. Introduction

Central nervous system (CNS) development is regulated by a complex interplay of chemical and mechanical factors, which direct neural progenitor cell (NPC) proliferation, migration, and differentiation through sequentially and spatially coordinated events. The first neural structure that arises in the embryo is the neural tube, which consists of a pseudostratified layer of neuroepithelial cells.[1] These early neural stem cells (NSCs) represent the founders of neurons, astrocytes, and oligodendrocytes.[2,3] Significant advances have been made in clarifying the chemical signals involved in neurodevelopment.[4–6] Starting with the formation of the neural tube, many mechanical events mark the major steps of CNS morphogenesis, such as the tube expansion, which then forms the three primary encephalic vesicles, neural migration, axon outgrowth, pathfinding, and gyrification of the cerebral cortex.[1,7] The role of mechanical cues is however still poorly understood[8] and is attracting attention.[9–12] Mechanical stimuli can be classified as passive and active which interplay during neurodevelopment.[13] Passive mechanical forces influence cells through matrix stiffness, porosity, and topography. The mechanical properties of the extracellular matrix change over time and space in the developing neural tissue,[14,15] and coordinate with chemical signaling cascades in building the CNS. Conversely, active stimulations are generated by tissue reshaping due to cell proliferation, migration, cell-cell, and cell-matrix adhesion. For example, in the neural tube or the cortex gyri, they generate and transmit over long distances, pulling and pushing forces that stretch, compress, bend or twist the surrounding cells.[9,16,17]

The effects of passive stimuli on NPC differentiation have been investigated above all using 2D and 3D scaffolds which can be precisely designed with tailored features.[18,19] Unfortunately, active forces are challenging to investigate because of the limited availability of biophysical tools to generate them in vitro and in vivo. Fire-polished glass pipettes have been used to influence NSC differentiation along a neuronal or astrocytic lineage by modulating the activity of stretch-activated ion channels.[20] Stretchable membranes actuated by a linear translation stage have been

applied to generate high mechanical tension in vitro for inducing NSC differentiation toward mature neuronal cells.[21,22]

Remotely controlled magnetic manipulation is now being used to generate active mechanical stimulations in neural cells.[23–28] The "nano-pulling" paradigm is based on cell loading with magnetic nanoparticles (MNPs) combined with a magnetic field gradient to generate a magnetic force. Since cells behave like a viscoelastic fluid, the magnetic force generated is likely to be dissipated through deformation, and the rigid elements of the cell cytoskeleton thus undergo stretching.

Magnetic nano-pulling allows the in vitro chronic stimulation of cells with extremely low forces (<1 nN) and continuous load application for days or weeks, mimicking in vivo developmental conditions. This process is named stretch growth (SG)[29] and is accompanied by the addition of new mass and axonal cytoskeleton remodeling.[28,30] In developing neurons, nano-pulling is associated with axonal elongation, sprouting, and neuron maturation.[25,28,30–33] This suggests that SG may also influence neurogenesis. Recently, magnetic nano-pulling was used to promote the neural differentiation of stem cells.[23] However, many questions remain open: i) Does the in vitro chronic application of extremely low active forces mimicking endogenous in vivo conditions influence NSC differentiation? In line with the effects observed in developing neurons, ii) is maturation affected? iii) Are the mechanisms behind SG conserved between different developmental stages, with similarities in the responses of immature and mature neurons? Finally, iv) can mechanical stimuli induce SG of neurons grafted into a nervous tissue?

To address these points, in this work, spinal cord (SC)-derived human neuroepithelial stem (NES) cells were used.[34,35] SC-NES cells show great neurogenic potential, generating mature neurons with extended complex neurites, as well as astrocytes and oligodendrocytes, thus demonstrating their multipotentiality. In addition, SC-NES cells injected in rodent models of spinal cord lesions can establish functional circuits leading to an amelioration of motor deficits,[34] thus showing great potential for the treatment of spinal cord injuries (SCI).

In this work, SC-NES cells were subjected to a standard differentiation protocol, in the presence or absence of nano-pulling. Nano-pulling was found to induce a strong remodeling at the level of the cytoskeleton, synapses, and neural network, thus reducing the time required for the maturation of neural precursors into mature neurons. The morphological and functional remodeling induced by nano-pulling matches our previous observations in hippocampal neurons.[28] This thus suggests that mechanosensitivity is a unified and well-conserved mechanism in development aimed at regulating neurogenesis and neuronal terminal differentiation. Lastly, our results support the hypothesis that nano-pulling can induce SG in the spinal cord tissue, thus opening up fascinating opportunities regarding the use of mechanical stimuli for the treatment of SCI.

2. Results

2.1. Nano-Pulling of SC-NES Cells Induces Stretch Growth

SC-NES cells were differentiated following a previously described protocol.[34] Briefly, cells were incubated in the pre-differentiation medium for seven days in vitro (DIV) and in the terminal differentiation medium from DIV7 up to DIV90, when they differentiate into mature neurons (**Figure 1**A). In order to test the best paradigm for MNP administration, SC-NES cells were loaded with MNPs 4 h after the beginning of the pre-differentiation phase (DIV0) or 4 h after the beginning of the differentiation phase (DIV7). At DIV8, both groups were exposed to the external magnetic field ("stretch" group) or placed in a mock apparatus producing a null magnetic field ("ctrl" group) for 48 h. A single-neural process tracing analysis was then performed on tubulin beta 3 (TUBB3)-positive cells (see Figure S1A, Supporting Information).

For both conditions, an increase in neural process length in the stretched group was observed but not in the control group ($p < 0.0001$, Figure S1B, Supporting Information). Specifically, the two loading protocols resulted in a length increase of $65.8 \pm 3.3\%$ and $75.7 \pm 3.8\%$ for DIV0 and DIV7, respectively, which was not statistically different between the two stretched groups ($p = 0.29$, Figure S1B, Supporting Information). This suggests that the time of MNP administration may not be crucial for nano-pulling to exert its effect on neural process lengthening. For the subsequent experiments, MNPs were added 4 h after the beginning of the differentiation phase (DIV7). MNPs alone or the magnetic field alone had no effects on the length of the neural processes (Figure S1C, Supporting Information).

2.1.1. Nano-Pulling Generates a Pico-Newton Force on Neural Processes

MNP degradation dynamics were characterized at different time points (1, 3, 7, and 10 days after MNP addition) by measuring the intracellular levels of Fe^{2+}/Fe^{3+}. In line with our previous data from mouse hippocampal neurons,[28,36] the intracellular iron level dramatically increased after 3 days from the MNP addition, marking the beginning of particle degradation in ionic Fe (Figure 1B1). MNP internalization was quantified at the same time points, as total iron with thiocyanate assay (Figure 1B2). Interestingly, both curves reached a plateau 7 days after MNP addition that is very similar (4–5 pg of Fe per cell), likely corresponding to a steady state in the dynamics of iron accumulation and elimination. In order to understand whether MNP internalization and degradation could affect cell viability, the fraction of cells positive to the apoptotic marker cleaved Caspase 3 (cCASP3) was quantified. No statistically significant difference was found comparing the two conditions, MNP+ and MNP−, for all the time points tested. The percentage of apoptotic cells was similar to the baseline level (MNP−, day 0 after MNP addition) ($p > 0.99$ for all conditions, Figure 1C). Moreover, to evaluate the effect of a long-term administration, the cCASP3 signal was quantified in DIV90 cells. The results confirmed our previous observations, showing no statistically significant difference between MNP+ and MNP− ($p = 0.37$), and both conditions were similar to the baseline level ($p = 0.94$ and $p = 0.22$ for MNP− and MNP+ respectively, Figure S2, Supporting Information).

MNP internalization and intracellular localization was studied by transmission electron microscopy (TEM) imaging at DIV7 and DIV10, by performing a short-time assay after
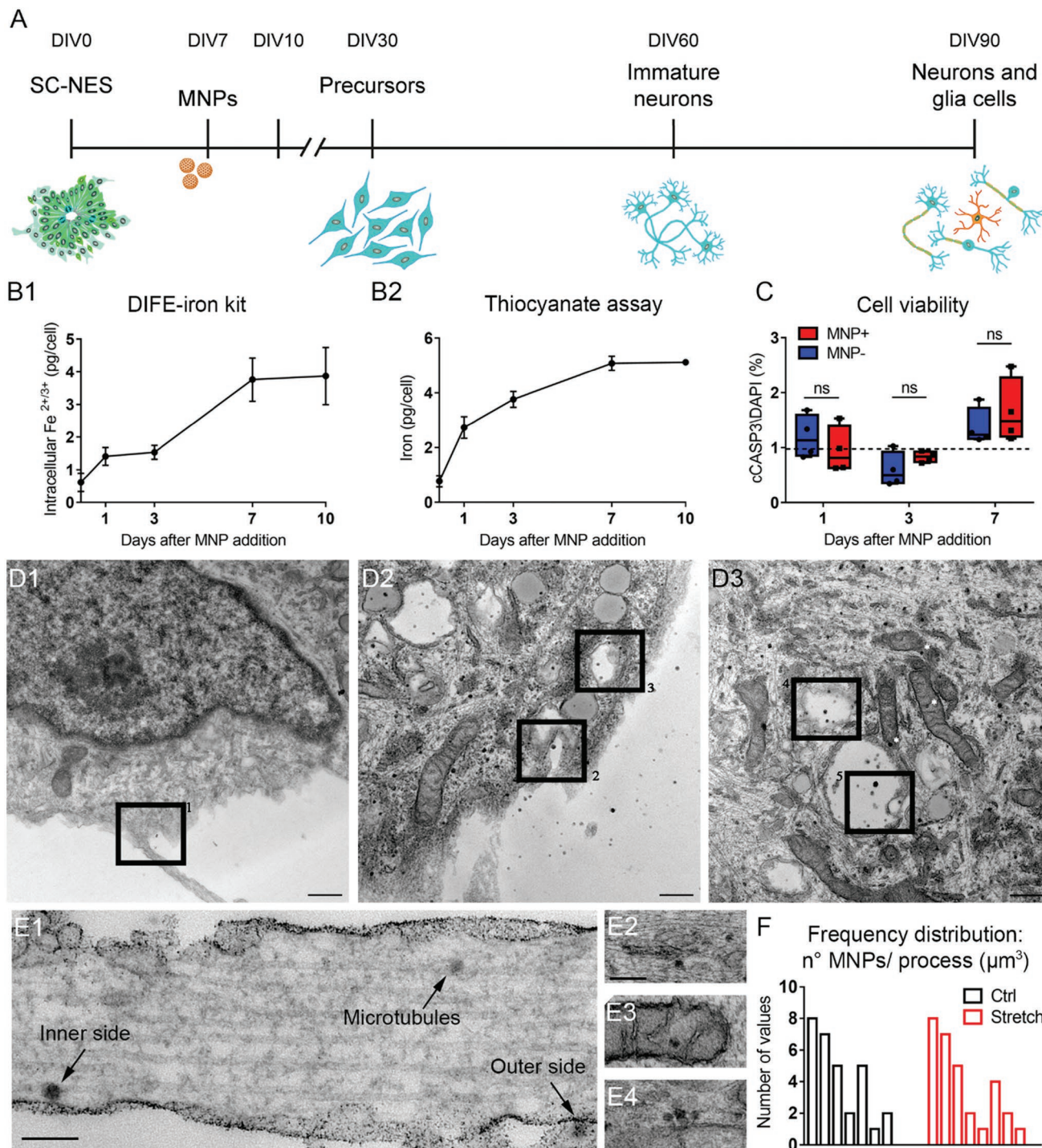
Figure 1. Loading of SC-NES cells with MNPs. A) Schematic representation of the differentiation protocol from undifferentiated SC-NES cells (DIV0) into neurons and glial cells (DIV90), with the addition of MNPs at DIV7. B1) Intracellular level of $Fe^{2+/3+}$/cell and B2) total iron/cell at different time points after MNP loading (0 time point); $n > 3$ replicates and $n = 2$ replicates, respectively. C) Analysis of cCASP3-positive cells. Box plot, min-to-max, $n > 1000$ cells, $n = 4$ replicates. Two-way ANOVA with Tukey's HSD post hoc test. Row factor (MNP^- vs MNP^+): $p = 0.0025$, $F = 8.53$. Columns factor (days after MNP addition): $p = 0.56$, $F = 0.34$. D) Representative TEM micrographs of internalization through ruffle-mediated micropinocytosis in NES cells at DIV7, after 30 min of incubation with MNPs. D1) MNPs in close proximity to a membrane ruffle, D2) MNPs in endosomes close to the cellular membrane, and D3) endosomes positive for MNPs internalization already far from the membrane. White stars highlight examples of mitochondria positive for MNPs. Scale bar 500 nm. E) Representative TEM micrographs of the localization of MNPs inside a neural process of a NES cell at DIV10. Scale bar 200 nm. E1) MNPs localize both in the outer and inner sides of the cellular membrane, as well as inside the cytoplasm, where, eventually, they are associated with microtubules and endoplasmic reticulum (E2), or inside mitochondria (E3) and a few clusters of 2–3 particles were observed (E4). F) Quantification of MNPs in the processes of DIV10 SC-NES cells in control and stretched conditions. Histogram of the frequency distribution, $n = 30$ processes, $n = 3$ replicates. Kolmogorov–Smirnov test, $p = 0.80$.

ADVANCED
SCIENCE NEWS
www.advancedsciencenews.com

NANO · MICRO
small
www.small-journal.com

incubating the cells for 30 min, 1 h, and 2 h with MNPs. After 30 min, MNPs were found in close proximity to membrane ruffles (box1, Figure 1D1) and in endosomes formed by membrane ruffles (box2-3, Figure 1D2), suggesting a micropinocytosis ruffles-mediated mechanism of internalization. Figure 1D3 shows in box4 an endosome located in the cytosol far from the outer cell membrane, suggesting the movement from the cellular periphery to the perinuclear region of endosomes positive for particles internalization. Moreover, box5 of Figure 1D3 shows a mature endosome containing several MNPs, suggesting its formation by fusion of smaller endosomes. White stars in Figure 1D3 show some mitochondria positive for MNPs. Indeed, in line with our previous results,[28,37] MNPs were found to be located in the neural processes at both the inner and outer sides of the cell membrane (Figure 1E1) and diffused within the cytoplasm, associated with microtubules (MTs) or endoplasmic reticulum (ER) and inside the mitochondria (Figure 1E1–E3).

Clusters of 2–3 particles (Figure 1E4) were rarely observed, indicating that MNPs are internalized as single particles. The number of MNPs was quantified in TEM images and normalized per unit of the neural process volume analyzed (1.72 ± 0.31 MNPs·μm^{-3}, $n = 30$). No differences were observed comparing the frequency of MNP distribution in control and stretched processes ($p = 0.80$, Figure 1F), meaning that nano-pulling does not alter the localization of the MNPs. The neural process was then modeled as a cylinder and the mean volume was calculated based on the mean length and caliber of control neural processes reported in the next section. Specifically, the mean total volume of MNPs in the neural process was found to be 4.24 ± 0.075 μm^3. Using Equation (1) (see Experimental Section), the mean force generated on-axis in the neural process was estimated to be 10.55 ± 1.85 pN.

2.2. Responsiveness of SC-NES Cells to Strech Growth Is Cell-Stage Independent

To test the responsiveness of SC-NES cells to SG during the differentiation process and to collect quantitative data, MNPs were added at different time points during terminal differentiation (DIV7, DIV27, DIV57, and DIV87) and cells were stimulated for the subsequent 48 h (**Figure 2**A). The SG of stretched samples was observed at all the time points tested ($p < 0.0001$, Figure 2A1–A4), demonstrating that cells respond to stretching throughout the process of cell differentiation. The increase in neural process length between the control and stretched conditions at DIV10 is easily detectable when cells are cultured in microfluidic devices. Specifically, the microfluidic system is composed of two chambers connected by microfluidic channels: cells are seeded in one compartment and neural processes can easily cross the channels and invade the opposite chamber. Under the effect of directional nano-pulling, stretched neural processes show a strong tendency to reach longer distances than the unstretched group (Figure 2B). However, the highest increase in neural process length was observed at DIV10 ($65.8 \pm 5.9\%$ at DIV10, $33.2 \pm 4.3\%$ at DIV30, $41.3 \pm 3.4\%$ at DIV60, and $53.5 \pm 4.2\%$ at DIV90; Figure 2C).

These results were not related to the specific NES cell line, since a similar outcome was observed in NES cells derived from human-induced pluripotent stem (iPS-NES) cells (Figure S3, Supporting Information).

At DIV10, process orientation was quantified as orientation index (OI) which was defined as OI = $\cos(\theta)$, with $0 < \theta < \pi$ (OI = 1 when the process has the same direction of the force and OI = 0 when the direction of the process is perpendicular to the direction of the force). In line with previous studies,[24,26,38,39] we found processes in stretched samples to be significantly more aligned to the force vector ($p < 0.0001$, Figure 2D).

2.3. Nano-Pulling Induces Accumulation of Microtubules, Mitochondria, and Endoplasmic Reticulum in Neural Processes

To demonstrate that the lengthening of the neural processes is an example of real growth rather than merely viscoelastic deformation, their caliber was estimated under the maximum elongation rate (i.e., DIV10, Figure 2E). No statistically significant difference was detectable between the control and stretched groups (p = 0.15), suggesting that mass addition may occur.

This prompted us to investigate the cellular mechanisms underlying this phenomenon by comparing the ultrastructure of control and stretched neural processes. TEM imaging was used to trace MTs and to estimate the linear density as the ratio of their number in a longitudinal cross-section to the neural process caliber (**Figure 3**A1). A strong increase in MT linear density was found (p<0.0001, Figure 3A2). Specifically, 2.8 ± 0.1 and 4.4 ± 0.1 MTs μm^{-1} were measured in control and stretched conditions respectively, with a net increase of ≈60%. Similarly, enrichment of ER cisternae was revealed in stretched samples by analyzing TEM images ($80.6 \pm 14.7\%$, $p < 0.0001$, Figure 3A3). The accumulation of ER was confirmed by immunostaining for KDEL (Figure 3B1), with an increase of $71.8 \pm 6.6\%$ in the stretch group versus the control group ($p < 0.0001$, Figure 3B2). Considering the role played by the ER in local lipid and protein production,[40] these results seem to support the hypothesis that new mass could be added locally in response to SG.

2.4. Nano-Pulling Shapes Cell Networking

Previous studies analyzing the effect of active force application have suggested that mechanical exogenous forces may act on NSC commitment, by enhancing the elongation and maturation of NSC-derived neurons.[21–23] Unlike previous reports, here, SC-NES cells were stimulated from the beginning to the end of the differentiation process, in order to fully describe the effects of SG at different time points. Specifically, cells were exposed to the stimulus for 8, 22, or 52 days after the beginning of the differentiation protocol (**Figure 4**A). Cells formed a complex network with interconnected neural processes (Figure 4B). The extension of neural processes for each soma was estimated as the ratio of the TUBB3-positive area by the number of somata in the region of interest (ROI).

Our data showed a statistically significant increase in the area occupied by neural processes per number of somata in stretched samples in comparison with the control (p < 0.0001,
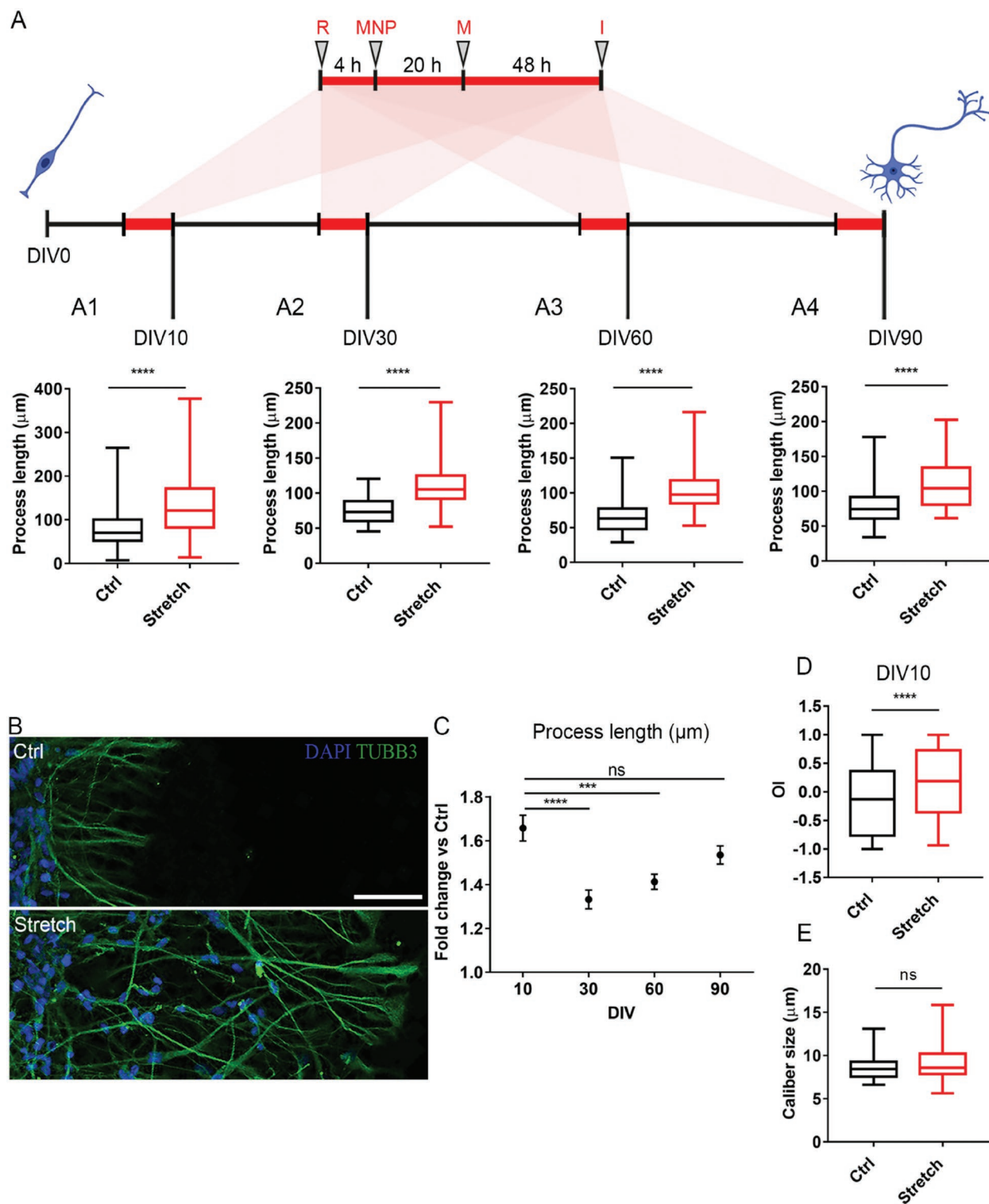
ADVANCED
SCIENCE NEWS
www.advancedsciencenews.com

NANO · MICRO
small
www.small-journal.com

Figure 2. Short-term stretching assay. A) Schematic representation of the short-term experimental design during the differentiation of SC-NES cells into neurons. At DIV7, 27, 57, and 87 cells are replated (R), 4 h later MNPs are added, and 20 h later the "stretch" groups are exposed to the magnetic field (M). After 48 h of continuous stretching, samples are fixed and subjected to imaging (I). A1) Neural process length at DIV10, $p < 0.0001$. A2) Neural process length at DIV30, $p < 0.0001$. A3) Neural process length at DIV60, $p < 0.0001$. A4) Neural process length at DIV90, $p < 0.0001$. A1–A4) Box plot, min-to-max, $n = 400$ processes, $n = 4$ replicates. Mann–Whitney test. B) Representative images of TUBB3 (green) and DAPI (blue) in control (upper part) and stretched (bottom part) conditions of NES cells cultured in microfluidic devices at DIV10. Scale bar 100 µm. C) Fold change comparison of stretched versus control conditions at different DIV. Mean ± SEM, $n = 400$ processes, $n = 4$ replicates. One-way ANOVA with Tukey's HSD post hoc test, $p < 0.0001$, $F = 9.89$. D) Orientation index distribution of neural processes at DIV10. Box plot, min-to-max, $n = 200$ processes, $n = 4$ replicates. Mann–Whitney test, $p < 0.0001$. E) Neural process caliber at DIV10. Box plot, min-to-max, $n = 40$ processes, $n = 4$ replicates. Mann–Whitney test, $p = 0.15$.
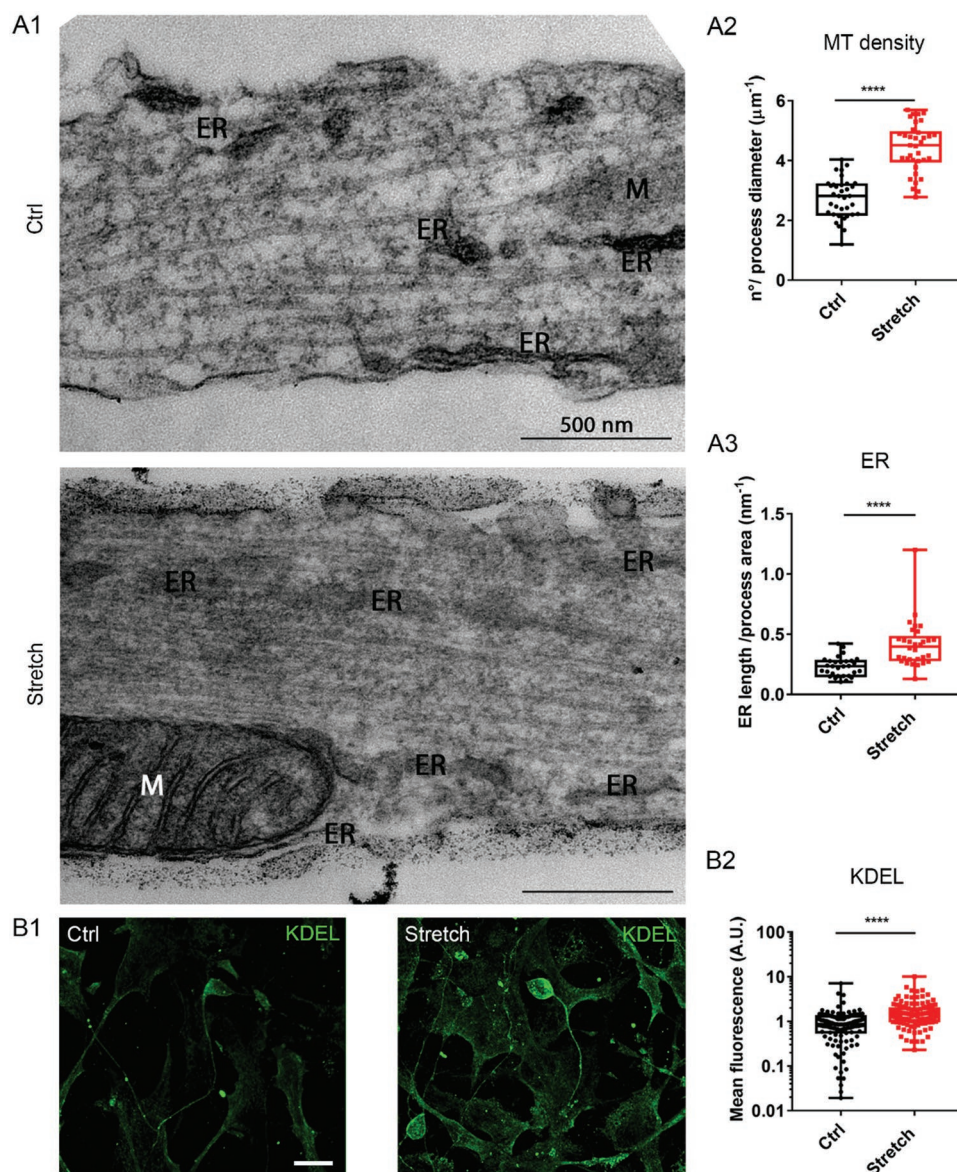
Figure 3. Enrichment of mitochondria, microtubules, and endoplasmic reticulum in stretched SC-NES cells. A1) Representative micrographs of SC-NES cells at DIV10 in control and stretched conditions. Mitochondria (M) and endoplasmic reticulum (ER) highlighted. Scale bar 500 nm. A2) Quantification of microtubule linear density. Box plot, min-to-max, all points, $n = 35$ processes, $n = 3$ replicates. T-test for unpaired data, $p < 0.0001$, $t = 9.496$, $df = 68$. A3) Quantification of ER cisternae. Box plot, min-to-max, all points, $n = 30$ processes, $n = 3$ replicates. Mann–Whitney test, $p < 0.0001$. B1) Representative pictures of SC-NES cells at DIV10 in control and stretched conditions stained with KDEL (green). Scale bar 10 μm. B2) Quantification of KDEL fluorescence. Box plot, min-to-max, all points, $n = 120$ processes, $n = 4$ replicates. Mann–Whitney test, $p < 0.0001$.

with an increase of 135.8 ± 6.8%, 72.4 ± 3.6% and 77.5 ± 3.9% after 8, 22, and 52 days of stretching, respectively, Figure 4C), while no differences were detected within the three control conditions ($p > 0.99$, $p = 0.86$, and $p > 0.99$ for MNP⁻M⁻ vs MNP⁺M⁻, MNP⁻M⁻ vs MNP⁻M⁺, MNP⁺M⁻ vs MNP⁻M⁺, Figure S4A, Supporting Information). To prove the effect of the stimulation on neural processes, phosphorylated histone H3 (pHH3) was quantified as a marker of cell proliferation. No statistically significant differences were observed between stretched and control groups ($p > 0.99$, Figure S4B, Supporting Information), testifying that the enhanced network formation is a consequence of nano-pulling. Cells thus responded

to continuous stimulation, even after prolonged exposure and irrespectively of their maturation stage. Interestingly, the elongation curves of control and stretched samples followed essentially the same trend (the curve shifts up) (Figure 4C). At the earliest time-point (DIV16), stretched samples showed a higher outgrowth rate than the controls (18.59 and 7.88 μm² day⁻¹, respectively, $p < 0.0001$, Figure 4D), but both groups reached a plateau at DIV30, with a null rate, likely due to the interconnection of the neural processes in a complex network formation (for both groups, $p < 0.0001$ between DIV16 and DIV30, and $p = 0.94$ and $p = 0.98$ between DIV30 and DIV60, for control and stretched groups respectively, Figure 4C).
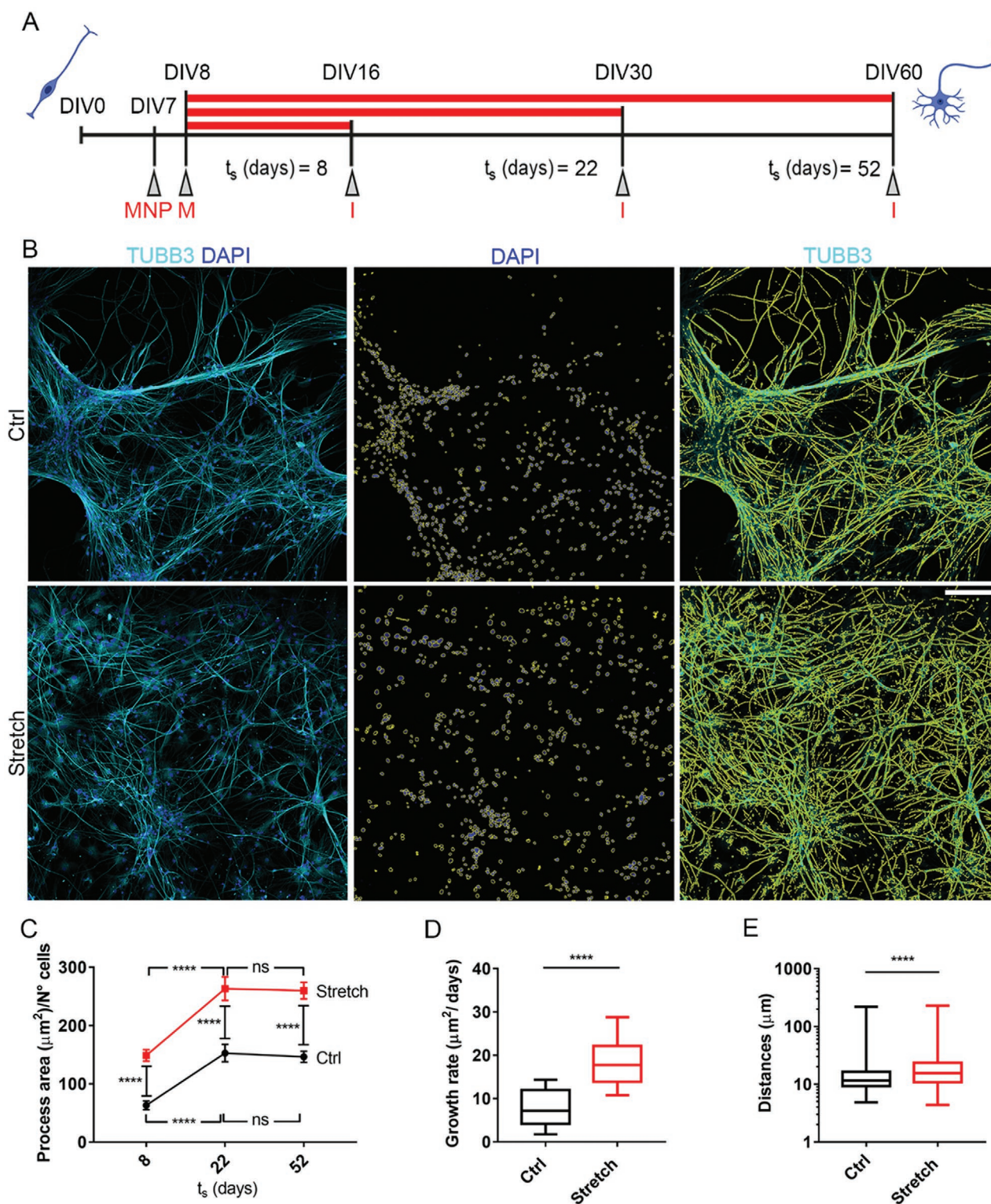
**ADVANCED
SCIENCE NEWS**

www.advancedsciencenews.com

NANO · MICRO
small

www.small-journal.com

Figure 4. Long-term stretching assay. A) Schematic representation of the long-term experimental design. At DIV7 MNPs are added and 20 h later the "stretch" groups are placed inside a magnetic applicator (M). After 8, 22, and 52 days of stretching, samples are fixed and subjected to imaging (I). t_s: stretching time. B) Representative images of TUBB3 (cyan) and DAPI (blue) in NES cells at DIV60 in the control and after 52 days of stretching. In yellow are the regions of interest of the occupied area. Scale bar 100 μm. C) Comparison between stretched and control conditions at different stretching times. Mean ± SEM, $n = 20$ pictures for each time point, $n = 4$ replicates. Two-way ANOVA test with Holm-Sidak post hoc's test. Row factor (Ctrl vs Stretch): $p < 0.0001$, $F = 37.17$. Columns factor (stretching time): $p < 0.0001$, $F = 89.53$. D) Analysis of growth rate after 8 days of stretching. Box plot, min-to-max, $n = 20$ pictures, $n = 4$ replicates. Mann–Whitney test, $p < 0.0001$. E) Analysis of nuclei dispersion at DIV60 ($t_s = 52$ days). Box plot, min-to-max, $n > 13474$ nuclei, $n = 4$ replicates. Mann–Whitney test, $p < 0.0001$.

ADVANCED
SCIENCE NEWS
www.advancedsciencenews.com

NANO · MICRO
small
www.small-journal.com

This raises the question as to whether interconnected neural processes can still respond to SG. At the last time-point (DIV60), the network morphology appeared to be considerably different between the two conditions (Figure 4B). It is well known that neuronal network morphology is strongly coupled with cellular connectivity[41] and that this kind of organization can occur in response to external stimuli.[42] This aspect was thus further investigated. By employing nuclei dispersion index $\overline{d}$ as an estimate of network morphology (Equation (2), see Experimental Section), a different data distribution was found ($p < 0.001$, Figure S4C, Supporting Information). A statistically significant increase of $28.7 \pm 0.2\%$ was detected in nuclei dispersion in stretched samples compared to controls ($p < 0.0001$, Figure 4E). This finding indicates that nano-pulling can alter the cell network formation.

2.5. Nano-Pulling Stimulates Neuronal Differentiation

The data collected raised the question as to whether the effects of the nano-pulling on network re-organization could also impact on neuronal differentiation processes. The cytoskeleton is subjected to changes during neurogenesis in cultured cells,[43] with early-stage cells containing only microfilaments, and MTs starting to appear at later stages. The cytoskeleton composition was thus evaluated through TEM analysis after seven days of stretching (DIV10, **Figure 5**A1–A4). An increase in the number of neural processes containing MTs was observed in stretched samples (ctrl: 46% of neural processes with microfilaments, 54% with microtubules; stretch: 20% with microfilaments, 80% with microtubules; $p = 0.0001$, Figure 5A5), supporting the idea that nano-pulling induces early remodeling of the cytoskeleton and speeds up the onset of neuronal differentiation.

In this regard, the mitochondrial pool is known to support neuron differentiation.[44,45] Specifically, variations in the mitochondrial pool correlate with the change in metabolism (from glycolytic to oxidative) that occurs during neuronal differentiation.[46] Here, TEM analysis showed that the number of mitochondria was significantly higher in the stretch group with respect to the control ($p = 0.006$, Figure 5A6).

To further confirm this result, the expression of SOX2 and RBFOX3 was studied at DIV30 and DIV60. SOX2 is a crucial transcription factor for the maintenance of stem cell multipotency whose expression wanes and eventually disappears during the completion of differentiation.[47] After 22 days of stimulation (DIV30), no differences in the percentage of SOX2 positive cells were observed between control and stretch groups while, after 52 days of stretching (DIV60), SOX2 staining still failed to show significant differences between control and stretch groups (DIV30: ctrl $81.5 \pm 17.4\%$, stretch $84.4 \pm 15.2\%$; $p = 0.92$; DIV60: $p = 0.99$; Figure 5B). Moreover, RBFOX3 (also known as NeuN), a common marker of mature neurons, showed low levels in both groups at DIV30 while a statistically significant increase in the number of RBFOX3 positive-cells was measured in the stretch group at DIV60, with $\approx 31.1 \pm 3.9\%$ of positive cells compared to $18.7 \pm 1.7\%$ of the control group ($p = 0.0008$, Figure 5C).

2.6. Nano-Pulling Stimulates Functional Neuronal Maturation

Data shown in Figure 5 raised the question as to whether long-term stimulation for up to 52 days could enhance the neuronal maturation process.

First, the mean fluorescence intensity of synaptophysin (SYP) immunoreactivity was measured in the control and stretched neural processes at different time points during the differentiation process (**Figure 6**A). The expression of this presynaptic protein was analyzed in order to evaluate the maturation level of the neuronal progeny[34,48] The temporal window of observation spanned from DIV16, when synapses are still immature, to DIV60, which is characterized by advanced synaptic maturation.[34] A statistically significant increase in SYP expression was observed in stretched samples after 8 days ($p = 0.0003$, Figure 6B) and 22 days ($p < 0.0001$, Figure 6C) of stimulation compared to the control cultures. On the other hand, at later stages of differentiation, after 52 days of stimulation (DIV60), no significant differences were detected between the stretch and control groups ($p = 0.91$, Figure 6D). A possible interpretation of these findings is that mechanical nano-pulling may simply speed up the maturation process.

To confirm this hypothesis, colocalization studies between a pre-synaptic and a post-synaptic marker were performed to estimate synapse density.[49,50] The colocalization between the presynaptic marker SYP and the postsynaptic marker HOMER1 was evaluated after 22 days of stretching (DIV30, Figure 6E). This time point was chosen because i) the difference in SYP expression between stretch and control groups showed the highest significance ($p < 0.0001$, Figure 6C), and ii) control cultures are expected to be in an immature stage.[51] A significant increase was observed in puncta showing apposition between SYP and HOMER1 spots, which reflects an increase in fully formed synaptic density, in stretched samples compared to the controls ($p < 0.0001$, Figure 6F).

To obtain functional evidence of the maturation boost induced by nano-pulling, patch-clamp recordings were employed to assess cellular excitability upon cell depolarization via positive current injection. At DIV30, no action potentials were elicited. In DIV60 cultures, stretched cells fired a higher number of action potentials than control cells, while at DIV90 no difference was detected between the two groups (**Figure 7**A,B). Spontaneous activity in the absence of membrane depolarization was then recorded. At DIV60, 42.3% of stretched cells and 24.0% of control cells showed spontaneous action potentials (Figure 7C). Interestingly, at DIV90 this trend reached statistical significance, with 68.2% of stretched cells showing spontaneous action potentials, in comparison to 23.8% of control cells (Figure 7C). On the other hand, no significant differences in resting membrane potential were observed (Figure 7D).

Overall, these results agree with an accelerated path of SC-NES cells toward a fully functional neuronal phenotype.

2.7. Nano-Pulling Induces SG of NES Cells Transplanted into the Spinal Cord Tissue

An organotypic co-culture model was generated by engrafting SC-NES cells into the ventral horns of day ex vivo (DEV)
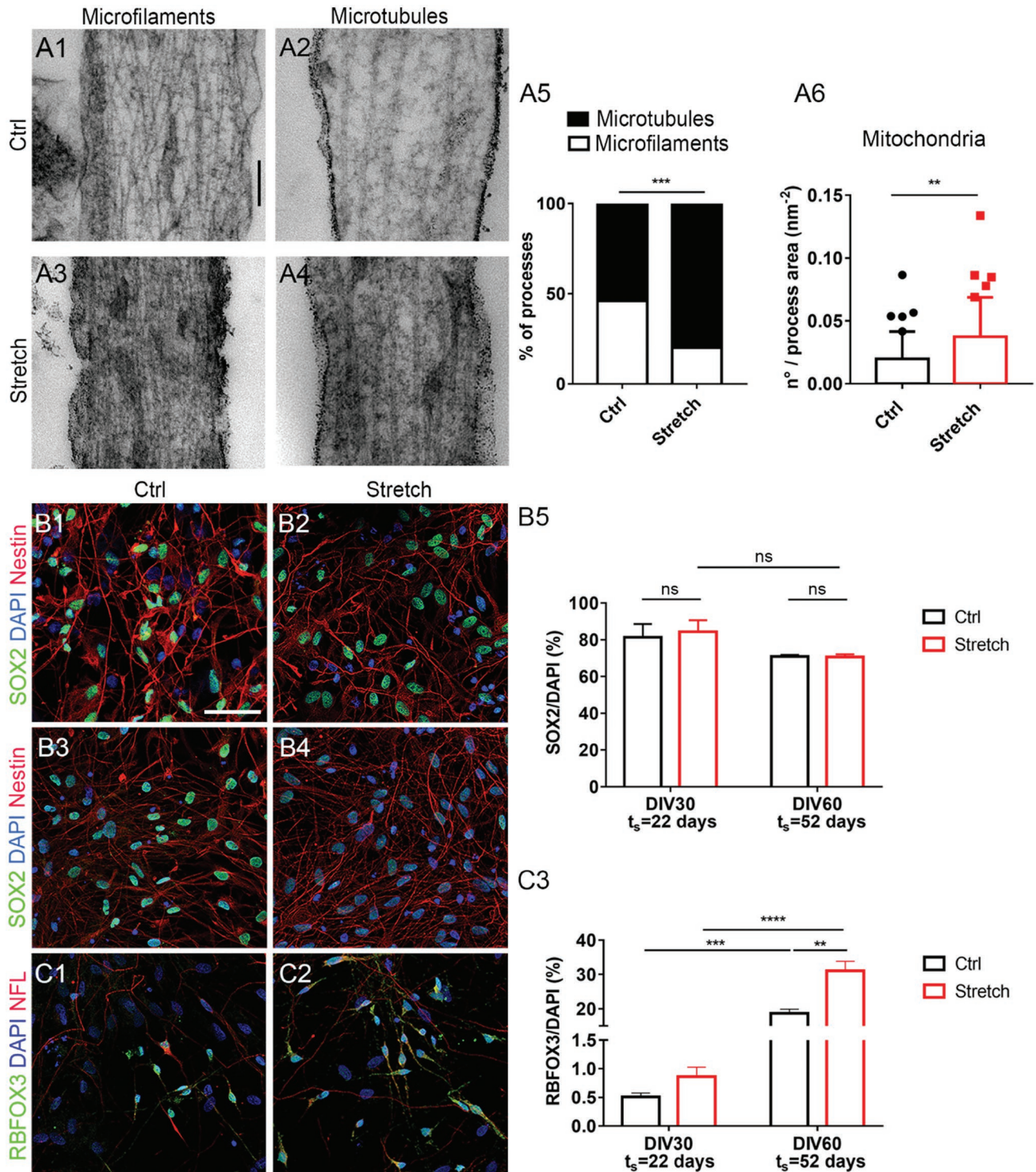
Figure 5. Effect of low forces on the differentiation of SC-NES cells into neurons. A1–A4) Representative micrographs of microfilaments and microtubules in control and stretched samples at DIV10 (A1–A2 and A3–A4, respectively). Scale bar: 200 nm. A5) Quantification of the cytoskeletal composition. Fisher's test, $n = 50$ neural processes, $n = 3$ replicates, $p = 0.0001$. A6) Quantification of the number of mitochondria. Box plot, 5–95 percentile, $n = 100$ processes, $n = 3$ replicates. Mann–Whitney test, $p = 0.006$. B1–B4) Representative pictures of SOX2 (green), DAPI (blue), and hNestin (red) immunofluorescence in control (ctrl) and stretched (stretch) cells at DIV30 (B1–B2, respectively), and at DIV60 (B3–B4, respectively). Scale bar: 50 μm. B5) Analysis of SOX2- positive cells at DIV30. Mean ± SEM, $n > 1000$ cells, $n = 3$ replicates. Two-way ANOVA with Tukey's HSD post hoc test. Row Main factor 1 (ctrl vs stretch): $p = 0.10$, $F = 3.07$. Main columns factor 2 (days of stretching): $p = 0.85$, $F = 0.04$. C1,C2) Representative pictures of RBFOX3 (green), DAPI (blue), and neurofilament (NFL, red) immunofluorescence at DIV60 in control and stretched conditions. C3) Analysis of RBFOX3-positive cells. Mean ± SEM, $n > 1000$ cells, $n = 3$ replicates. Two-way ANOVA with Tukey's HSD post hoc test. Row factor (ctrl vs stretch): $p < 0.0001$, $F = 453.7$. Columns factor (days of stretching): $p = 0.0014$, $F = 31.19$.
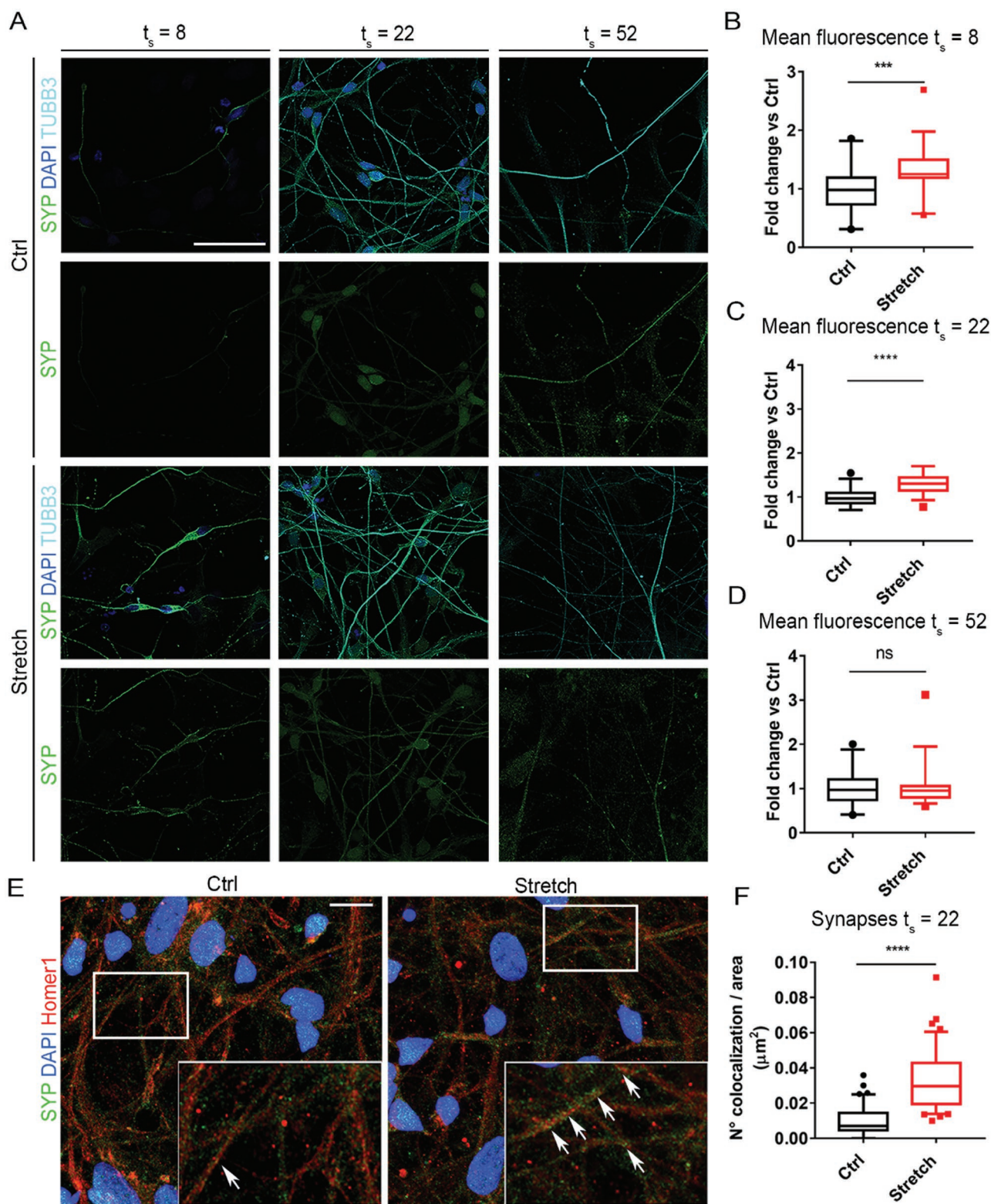
Figure 6. Effects of low forces on neuronal maturation. A) Representative pictures of SYP (green), DAPI (blue), and TUBB3 (cyan) in control and stretched conditions at $t_s = 8$ (DIV16), $t_s = 22$ (DIV30), and $t_s = 52$ (DIV60). Scale bar 50 µm. B) Analysis of SYP mean fluorescence in neural processes at $t_s = 8$, Mann–Whitney test, $p = 0.0003$. C) Analysis of SYP mean fluorescence in neural processes at $t_s = 22$, t-test for unpaired data, $p < 0.0001$. D) Analysis of SYP mean fluorescence in neural processes at $t_s = 52$, Mann–Whitney test, $p = 0.91$. B–D) Box plot, 5–95 percentile, $n = 36$ pictures, $n = 4$ replicates. E) Representative pictures of SYP (green), DAPI (blue), and Homer1 (red) in control and stretched conditions at $t_s = 22$. White arrows point to the colocalization spots of SYP and Homer1. Scale bar 20 µm. F) Quantification of the colocalization. Box plot, 10–90 percentile, $n = 40$, $n = 4$ replicates. Mann–Whitney test, $p < 0.0001$. t_s: stretching time.
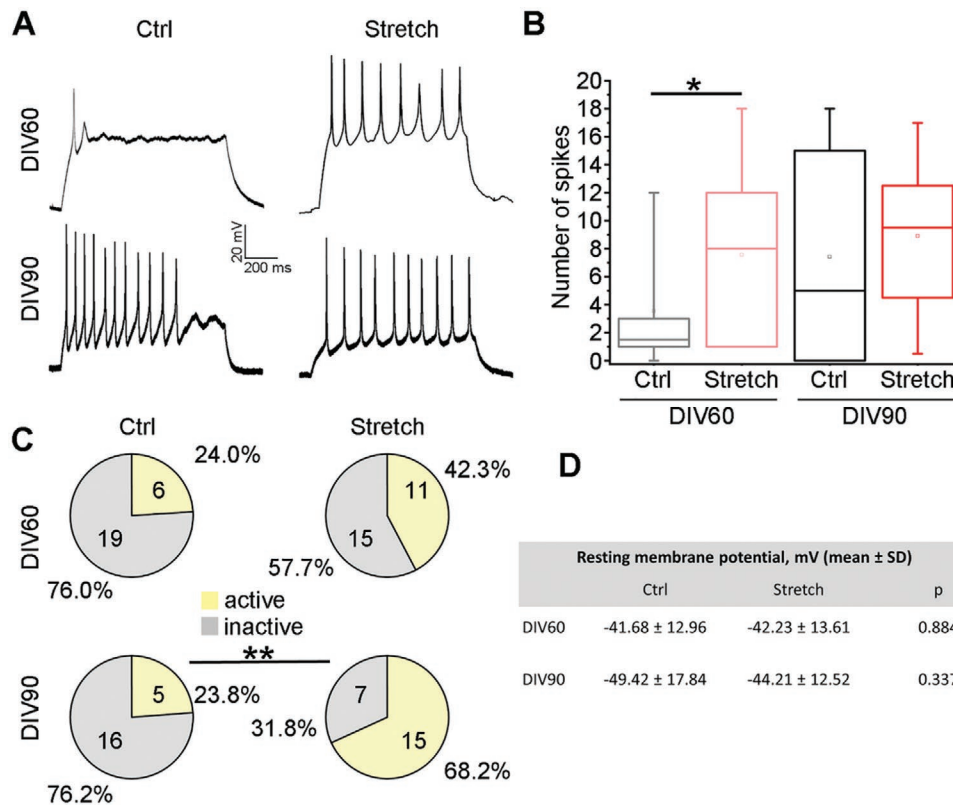
Figure 7. Patch-clamp recordings on SC-NES cell-derived neurons subjected to nano-pulling. A) Representative traces from current clamp recordings of SC-NES cells. B) Quantification of the number of action potentials fired by cells in response to a depolarizing current step (DIV60-ctrl, $n = 22$; DIV60-stretch, $n = 23$; DIV90-ctrl, $n = 19$; DIV90-stretch, $n = 20$; Mann–Whitney rank sum test, $*p = 0.029$). C) Pie charts showing the percentage of neurons showing spontaneous action potentials; numbers in each sector report the size of each group (Fisher exact test, DIV60, $p = 0.237$, DIV90, $**p = 0.006$). D) Table showing no significant difference in the resting membrane potential of cells (DIV60-ctrl, $n = 25$; DIV60-stretch, $n = 26$; Student's t-test; DIV90-ctrl, $n = 21$; DIV90-stretch, $n = 22$; Mann–Whitney rank sum test). $N = 3$ replicates for DIV60 and DIV90.

4 mouse SC slices. First, we evaluated the viability of transplanted cells in the host tissue, according to the protocol reported in Figure S5, Supporting Information. 6 days after transplantation, the fraction of transplanted human cells positive to the apoptotic marker cCASP3 was $2.14 \pm 2.90\%$ ($n = 15$ slices, on average 500 cells per slice), showing an excellent viability. For the stretch-growth assay, DIV10 MNP-loaded and DiI-labelled human SC-NES cells were injected into the ventral horns of DEV4 mouse SC slices, according to the protocol shown in **Figure 8**A. SC-NES cells were successfully integrated into the SC slices at DEV7 (Figure 8B, see also the 3D reconstruction in Movies S1,S2, Supporting Information). SC slices were positioned in the millicell insert radially oriented in the ventral-dorsal direction, in order to be aligned to the direction of the force vector (Figure 8C). At DEV5, the co-cultures were exposed to the magnetic field (stretch) or to a null magnetic field (ctrl) for 48 h. The sprouting of the neural processes of the cells transplanted in the ventral horn of the SC slice was generally oriented in the direction of the dorsoventral axis (i.e., the force vector direction) in stretched co-cultures, but not in the unstretched ones (Figure 8D1).

The direction of hNestin-positive neural processes was analyzed (Figure 8D2, relative to the two representative images shown in Figure 8D1). In stretched co-cultures, neural processes exhibited a preferential orientation, corresponding to

the peak of the Gaussian function of the directionality histogram, as documented by the percentage of processes with this preferred orientation (76%) and goodness of fit (0.59). The angle $\hat{\theta}$ between the preferential orientation and the force vector was $< 4°$, showing a very high alignment. Conversely, no single preferential orientation for hNestin-positive processes was detected in controls, with a low (i.e., 20%) fraction of them being aligned to the force vector and a goodness of fit of 0.4. A quantitative single-tracing analysis was then performed on the neural processes of hNestin-positive cells transplanted into SC slices ($n > 15$ slices per group, Figure S6, Supporting Information). An increase in the length of neural processes in stretch versus control groups was observed (73.16 ± 3.08 μm and 115.40 ± 4.17 μm for ctrl and stretch groups, respectively, $p < 0.0001$, Figure 8E), resulting in a length increase of approximately 58% after 48 h of stretching. The distribution of orientation index (OI $= \cos \theta$) was then calculated, $\hat{\theta}$ being the angle between the orientation of a neural process and the force vector. The smaller the angle $\hat{\theta}$ (i.e., OI is approaching to 1), the more aligned to the force vector the process is. In line with previous work[24,37–39] and in vitro experiments on SC-NES cells ($p < 0.0001$, Figure 1D), a comparison of the data distribution showed a statistically significant increase in the OI in the stretched versus unstretched condition ($p < 0.0001$, Figure 8F).
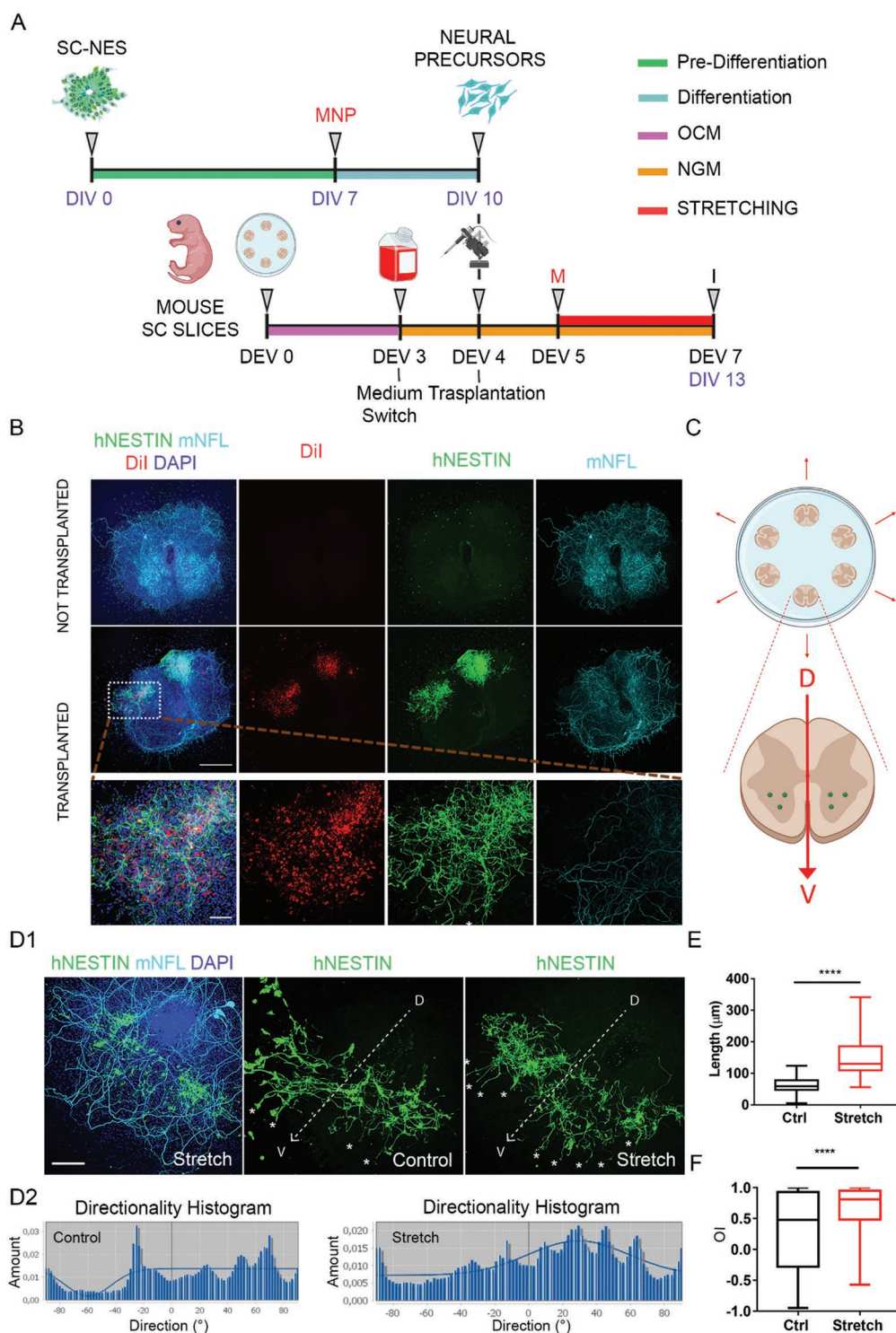
Figure 8. Nano-pulling of human SC-NES cells transplanted into mouse SC organotypic slices. A) Schematic representation of the transplantation protocol of human SC-NES-derived neural precursors loaded with MNPs into mouse SC slices. SC-NES cells are labelled with DiI before transplantation. B) Representative image of SC slices transplanted with SC-NES cells and not-transplanted (hNestin, green; DiI, red; m-NFL, cyan) (DEV10). Scale bars: 500 µm and 100 µm. C) Schematic representation of co-culture design: up to 6 SC slices are placed concentrically in a millicell with the dorso-ventral axis (red arrow) in the radial direction (centrifugal) and SC-NES cells are transplanted in the ventral horns (3 injections per horn). D1) SG of SC-NES cell-derived neural precursors inside the SC slices (hNestin, green; m-NFL, cyan; DAPI, blue). The white arrows show the dorso-ventral axis of the slice. The white stars highlight the presence of processes following a dorso-ventral axis orientation matching the force vector direction. Scale bar: 250 µm. D2) Directionality histograms for the representative stretched and control co-cultures shown in panel D1. E) Length and F) OI of the neural processes sprouting out from the SC slices at DIV 13–14 in stretch and ctrl groups ($n = 161$ processes, $n = 15$ slices, $n = 4$ mice). Mann–Whitney test, $p < 0.0001$. OCM: organotypic culture medium, NGM: neural growth medium (see Experimental Section).

**ADVANCED
SCIENCE NEWS**

www.advancedsciencenews.com

**NANO · MICRO
small**

www.small-journal.com

3. Conclusion

In this study, by generating active mechanical stimuli, we investigated the involvement of the force in the establishment of neuronal cell maturation and differentiation. Our stretching method is based on cell loading with MNPs. MNPs are internalized by a micropinocytosis ruffles-mediated mechanism of internalization and diffused within the cytoplasm (associated with MTs or organells, Figure 1D,E), where they generate a dragging force under an external magnetic field.

The net applied force was estimated to be around 10 pN in a cellular process with a length in the order of 100 μm. With such a small force, a constant load can be applied for hours to months. This makes our method an extraordinary tool for mimicking in vitro and ex vivo the condition of continuous loading with the extremely low forces that occur during development.

Short-term stimulation (48 h) was found to induce a strong elongation which reached the maximum rate of 0.20 ± 0.01 μm h^{-1} pN^{-1} when NES cells were stimulated between DIV8-10. The elongation took place without thinning (Figure 2D), indicating that the process is accompanied by the addition of mass.

The same methodology applied to hippocampal neurons was found to induce axon lengthening at a rate of 0.66 ± 0.02 μm h^{-1} pN^{-1}.[28] The similarity of the response to stretching between mature and immature neurons is not only in terms of elongation. In fact, ultrastructural analyses of immature neural processes of stretched NES cells showed an increase in the linear density of MTs, in the number of ER cisternae, and the number of mitochondria. These data are similar to findings previously reported for the stretched axons of mouse hippocampal primary neurons.[28,30,32]

This analogy across different stages of neural development raises the question as to how mechanical stimuli represent a well-conserved mechanism to shape the formation of the CNS during development. The observations collected in different models[28,30,37] and with different stretching modalities[28,32] consistently indicate the importance of MTs as a node in signal transduction. MTs of stretched processes are normal in structure but show a statistically significant increase in their density ($p < 0.0001$, Figure 3A). MTs behave like tension sensors,[52] which self-reorganize in the direction of maximal stretch and are stabilized by the application of a tensile force.[53] In light of this evidence, we speculate that nano-pulling is perceived by the mechanosensitive MTs, resulting in the stabilization of long stationary MTs.[30] A connection between an increase in MT density and mass addition is expected, considering that MTs are the tracks of axonal transport.

During the development of the neural processes of animal cells, peripheral ER usually co-aligns with MTs,[54–56] showing features such as anterograde and retrograde transport along axonal MTs. As expected, stretched neural processes showed a significant accumulation of tubular ER ($p < 0.0001$, Figure 3A3 and 3B2), similarly to previous observations on hippocampal neurons.[28,30,32] Furthermore MT-based transport of mitochondria into neural processes could explain the observed increase in the number of mitochondria found in the stretched neural processes of human NES cells (Figure 3A2), as previously reported for mouse primary neurons.[30] Our TEM data on NES cells also suggest that, although the mitochondrial morphology is quite similar in the two experimental classes, their length slightly, but significantly, increases upon SG. Together with mitochondria, ER plays a key role in the biosynthesis and calcium buffering in neural processes, which supports axonal transport and mass addition.[57] Since MT dynamics are also coupled to the axonal transport of vesicles,[58] an increase in the total number of available tracks is likely directly correlated with an increase in the total number of transported vesicles. Quantification of vesicles positive to the pre-synaptic marker SYP was performed to support this hypothesis. Pre-synaptic proteins are generally transported in the form of precursor vesicles from the neuronal soma, where they are synthetized, along axonal MTs to the synaptic terminal, where they anchor.[59] An increase in the signal was found after 8 and 22 days of stretching ($p = 0.0003$ and $p < 0.0001$, Figures 6B and 6C, respectively) which reached a plateau after 52 days of stretching ($p = 0.91$, Figure 6D).

In the light of these observations, we tested the effect of long-term stimulation in depth, by applying a continuous loading for up to 82 days. Long-term stimulation was found to induce remodeling of the cell network (Figure 4), which was accompanied by functional changes. Specifically, the colocalization between pre- and post-synaptic markers, considered a hallmark of the presence of mature synapses, showed a strong increase after 22 days of stimulation (p < 0.0001, Figure 6A–D). In line with this, TEM imaging revealed an increase in the number of neural processes containing MTs (p = 0.0001, Figure 5A1–4) in stretched cells, indicating later stages of in vitro neurogenesis.[43]

These results were confirmed by electrophysiological recordings that showed an increase in the number of spikes after 82 days of stretching, reaching a plateau after 90 days of stretching ($p = 0.029$, Figure 7B). In fact, the expression of synaptic markers and synapse density was high at early stages (DIV30) of maturation, while induced spiking activity increased at an intermediate stage (DIV60). This mismatch agrees with observations on human stem cell-derived neurons, in which synaptogenesis and structural modifications of the synapse precedes the acquisition of synaptic function.[60–62] At DIV90, the difference in terms of percentage of neurons showing spontaneous action potentials reached statistical significance ($p = 0.006$, Figure 7C). Interestingly, the mechanical stimulation not only speeds up neuronal maturation but also modulates the neuronal fate, as highlighted by the increase in RBFOX3-positive cells after 52 days of stretching ($p = 0.0008$, Figure 5B3).

Previous studies analyzing the effect of active force application suggested that mechanical passive and active forces may act on the neurodevelopmental trajectories of NSCs by accelerating the maturation of the derived neurons.[21–23] Here, a chronic stimulation was performed for up to 82 days which clearly demonstrated that mechanical stimulation can approximately halve the time required in vitro for the differentiation of neural precursor cells into mature neurons, thus also increasing the number of differentiated cells.

Although the picture is not yet complete, a crucial point arising from current and previous studies[28,30,32,37] is that mechanical stimulation is a well-conserved mechanism that induces a local remodeling in the neural process cytoskeleton. This then triggers the transport and localization of components involved in neural outgrowth, differentiation, and synapse maturation.

ADVANCED
SCIENCE NEWS
www.advancedsciencenews.com

NANO · MICRO
small
www.small-journal.com

As a final phase of this work, experiments were designed to assess the translational potential of the nano-pulling protocol by addressing the complexity of a neural tissue in an ex vivo paradigm. We used an organotypic model consisting of SC slices,[32,63,64] onto which we transplanted MNP-loaded human SC-NES cells. After cell engraftment, the co-culture was subjected to nano-pulling, demonstrating that the mechanical stimuli externally applied can induce the guided outgrowth of the neural processes of transplanted NPCs in this complex neural tissue environment. Specifically, the stretched processes showed a strong increase in the elongation rate (2.40 µm h^{-1} vs 1.52 µm h^{-1} of the control group) and a strong change in the OI, with the stretched processes preferentially aligned in the direction of the force vector (Figure 8E). We speculate that nano-pulling could be explored for the potential application in cell therapies, considering that it not only hastens the time needed for neuronal maturation but also modifies cell behavior. We are currently testing its use in pre-clinical models of SCI as a strategy to stimulate SC-NES cell differentiation into mature neurons and thereby to increase the efficiency of their integration into lesioned spinal circuits.

4. Experimental Section

Ethical Statement: All NES cell works were performed according to NIH guidelines for the acquisition and distribution of human tissue for bio-medical research purposes and with approval by the Human Investigation Committees and Institutional Ethics Committees of each institute from which samples were obtained. Final approval from the Committee on Bioethics of the University of Pisa was obtained (Review No. 29/2020). De-identified human specimens were provided by the Joint MRC/Wellcome Trust grant (099175/Z/12/Z), Human Developmental Biology Resource (www.hdbr.org). Appropriate informed consent was obtained, and all available non-identifying information was recorded for each specimen. Tissue was handled in accordance with ethical guidelines and regulations for the research use of human brain tissue set forth by the NIH (http://bioethics.od.nih.gov/humantissue.html) and the WMA Declaration of Helsinki (http://www.wma.net/en/30publications/10policies/b3/index.html).

Animal procedures were performed in strict compliance with protocols approved by Italian Ministry of Public Health and the local Ethical Committee of University of Pisa, in conformity with the Directive 2010/63/EU (project license no. 39E1C.N.5Q7 released on 30/10/2021). C57BL/6J mice were kept in a regulated environment (23 ± 1 °C, 50 ± 5% humidity) with a 12 h light–dark cycle with food and water ad libitum.

Maintenance and Differentiation of NES Cell Lines: Human SC-NES cells were previously derived as already reported from developing spinal cord tissue[34,35] and iPS-NES cells were derived from human induced pluripotent stem cells (hiPSCs) as already reported.[35,65,66] Briefly, hiPSCs were dissociated into single cells in StemFlex medium (#A3349201, Thermo Fisher Scientific, Waltham, Massachusetts)] in Matrigel coated dishes containing 10 µM Y-27632 (#72308, StemCell Technologies, Vancouver, Canada), until confluent. Then, the dual SMAD inhibition protocol was performed, changing the StemFlex medium with a neural induction medium [1:1 Dulbecco's minimum essential medium/F12 (DMEM/F12) (#11330-032, Gibco, Waltham, Massachusetts)) and Neurobasal medium (#21103-049, Gibco) with addition of B27 supplement (1:50, #175040-44, Gibco), N2 supplement (1:100, #17502-048, Gibco), 20 µg mL^{-1} insulin (#I9278, Sigma, St. Louis, Missouri), L-glutamine (1:100, #25030-081, Gibco), MEM non-essential amino acids (1:100, #11140-050, Gibco), and 2-mercaptoethanol (1:1000, #21985, Gibco)], supplemented with 100 nM of LDN-193189 (# 72144, StemCell Technologies), 10 µM of SB-431542 (#616464-5MG, Merck, Darmstadt,

Germany), and 2 µM of XAV939 (#72674, StemCell Technologies). The medium was changed daily until day 11. At day 12, the cells were dissociated with Accutase and maintained in the NES medium (DMEM/F12 with addition of B27 supplement (1:1000), N2 supplement (1:100), 20 ng mL^{-1} FGF-2 (#13256029, Gibco), 20 ng mL^{-1} EGF (#PHG0311, Gibco), 1.6 mg mL^{-1} glucose, 20 µg mL^{-1} insulin, and 5 ng mL^{-1} BDNF (#PHC7074, Gibco)) with Y-27632 (10 µM).

Concerning, the NES cells, they were maintained in NES medium. Cells were cultured in T25 flasks coated with POLFN [0.01% poly-L-ornithine (#P4957, Sigma), 5 µg mL^{-1} laminin (#23017-015, Invitrogen, Waltham, Massachusetts), and 1 µg mL^{-1} fibronectin (#354008, Corning, Corning, New York)] and maintained at 37 °C in a saturated humidity atmosphere of 95% air and 5% CO$_2$. Cells were split 1:2 when confluent (≈0.5–1 × 10^5 cells cm^{-2}), once every 4–6 days with 0.25% trypsin. Half volume of the medium was changed every 2–3 days.

Neuronal differentiation of NES cells was performed in two steps. For the pre-differentiation step, cells were seeded in NES medium without FGF-2 and EGF for 7 days, changing the medium every 2–3 days. For the terminal differentiation, cells were dissociated and replated at a density of 0.8–1 × 10^5 cells cm^{-2} in a medium composed of DMEM/F12 (1:2), Neurobasal (1:2), N-2 (1:200), B-27 (1:100), Insulin (10 µg mL^{-1}), L-glutamine (1:100), and BDNF (30 ng mL^{-1}). Half volume of the medium was changed every 2–3 days and neurons were differentiated up to 4 months.

Organotypic Model: An organotypic mouse model consisting of spinal cord slices was used, as previously described.[32,63,64] Spinal cords of P3 mice were dissected under a stereomicroscope in a solution of D-glucose 6.5 mg mL^{-1} in DPBS (#14190-094, Gibco), sliced (300 µm thickness), and placed on a Millicell membrane (#PICM0RC50, Merck), previously coated with a water solution of 0.1 mg mL^{-1} collagen (#C7661, Merck), 0.01 mg mL^{-1} poly-L-lysine (#P4707, Merck), and 0.01 mg mL^{-1} laminin (#L2020, Merck). Then, the SC slices were initially cultured in the organotypic culture medium (OCM) composed of MEM with 25% of horse serum, HBSS and HEPES, 35 nM of D-glucose, 1% penicillin, 1% streptomycin, and 2 mM of Glutamax and 0.1 µg mL^{-1} GDNF (#SRP3200, Merck).[67]

NES cells at early stages of differentiation (DIV10) were grafted in the ventral horns of the SC slice at DEV 4. Before grafting, NES cells were stained with 1 µg mL^{-1} DiI red dye (#C7001, Invitrogen) (5 min incubation at 37 °C, 15 min incubation at 4 °C). After washing with DPBS, cells were detached, counted, and resuspended at a concentration of 50 cells nL^{-1} in neuronal growth medium (NGM), composed by Neurobasal, N2 (1:100), B27 (1:50), Insulin (10 µg mL–1), l-glutamine (1:100), 1% penicillin, 1% streptomycin, and GDNF (100 ng mL^{-1}). 4 nL of cell suspension were transplanted into six locations for each slice (3 injection sites for each ventral horn). Then, SC slices were incubated in NGM and fixed at DEV7.

MNPs and Magnetic Field: MNPs used in this study were magnetite MNPs (#4115, Chemicell, Berlin, Germany) with a core of iron oxide ≈75 ± 10 nm in diameter and saturation magnetization of 59 Am^2 kg^{-1}, as stated from the supplier. The outer layer was made of glucuronic acid and the hydrodynamic diameter is 100 nm. The intracellular iron was quantified with an iron assay kit (#DIFE-250, BioAssay Systems, Hayward, California), and the absorbance was measured at a wavelength of 590 nm. Total iron was quantified via thiocyanate assay, incubating the cells with HCl 6 M and HNO$_3$ 65% for 1 h at 60 °C and diluting the samples in 1.5 M KSCN. The absorbance was measured at a wavelength of 478 nm.

Experiments were conducted in 35 mm Petri dishes placed inside a Halbach-like cylinder magnetic applicator, which provided a constant magnetic field gradient of 46.5 T m^{-1} in the radial centrifugal direction.[27,37] At DIV10, the force generated by MNPs was estimated by using the formula described in:[27]

$$F = \rho V M_s \nabla \vec{B} \tag{1}$$

with ρ being the density of iron oxide in the MNP core, V the total volume occupied by the iron core of the MNPs in the neural process, M_s the saturation magnetization, and $\nabla \vec{B}$ the magnetic field.

ADVANCED
SCIENCE NEWS

www.advancedsciencenews.com

NANO · MICRO

small

www.small-journal.com

Stretching Assay: Two different protocols of stretching were carried out. For the short-term assay cells were dissociated and replated at a density of 1×10^5 cells cm^{-2} in ibidi dish (#80416, IBIDI, Gräfelfing, Germany) precoated with Matrigel (1:60) or POLFN at DIV10, 30, 60, and 90. Alternatively, at DIV10, for confocal and electron imaging, $1-0.5 \times 10^5$ cells cm^{-2} were seeded on a 8 mm glass coverslips (#CB00080RA120MNZ0, Epredia, Portsmouth, New Hampshire), on Ibidi dishes with cell location grids ((#80156, IBIDI, Gräfelfing, Germany) or 2×10^5 cells in microfluidic XONA devices (#RD150, XONA, Research Triangle Park, North Carolina) mounted on 22 glass coverslips (#vntondi.22, F. Franceschini s.a.s., Pisa, Italy) pre-coated with 500 µg mL^{-1} poly-L-lysine (#P4707, Merck) and 0.01 mg mL^{-1} laminin (#L2020, Merck). 5 µg mL^{-1} of MNPs were added 4 h after seeding. 20 h later, the Petri dish (stretch group) was put inside the magnetic applicator or kept outside (ctrl group). After 48 h of stretching, samples were fixed and stained for 15 min with 0.1% vol/vol crystal violet in ethanol 10% or, alternatively, processed for immunofluorescence or electron microscopy.

For the long-term assay, cells were seeded for the terminal differentiation at a density of 0.5×10^5 cells cm^{-2} on 8 mm glass coverslips precoated with POLFN. 5 µg mL^{-1} of MNPs were added 4 h after seeding and, then, every 15 days up to 4 months. 20 h after MNP's addition, the Petri dish (stretch group) was put inside the magnetic applicator, keeping outside the control dish (ctrl group). After 8, 22, 52, and 82 days of stretching samples were electrophysiologically recorded or fixed and stained for immunofluorescence.

For the organotypic model, 4–6 slices were placed in a millicells with the dorsal-ventral axis in the radial direction (outward orientation) (Figure 8C).

Immunostaining: YFor immunostaining, NES cells were washed with DPBS and fixed with 4% formaldehyde (FA) for 12 min at room temperature (RT). After three washes of 3 min with DPBS-Triton X-100 (PBSX) (0.1% vol/vol Triton X-100 in DPBS Ca^{2+}/Mg^{2+} 1X), samples were permeabilized with permeabilization solution (0.5% vol/vol Triton X-100 in DPBS Ca^{2+}/Mg^{2+} 1X), and blocked at RT for 1 h with blocking solution (5% fetal bovine serum, 0.3% (vol/vol) Triton X-100 in DPBS Ca^{2+}/Mg^{2+} 1X). Primary antibodies were diluted in antibody solution (3% fetal bovine serum, 0.2% (vol/vol) Triton X-100 in DPBS Ca^{2+}/Mg^{2+} 1X) and incubated overnight at 4 °C. Primary antibodies were diluted as follows: TUBB3 (1:500, #T8578, Sigma), cCASP3 (1:200, #AB3623, Millipore), SYP (1:500, #Mab329, Millipore, Burlington, Massachusetts), Homer1 (1:350, #160023, Synaptic System, Göttingen, Germany), KDEL (1:200, PA1-013, Invitrogen), SOX2 (1:400, ab5603, Millipore,) RBFOX3 (1:500, #ABN78, Millipore), pHH3 (1:2000, 14955 Abcam), NFL (1:200, #2424662, Millipore), and Nestin (1:200, MAB1259, R&D, Minneapolis, Minnesota). The next day, samples were washed three times for 3 min and then incubated 1 h at RT with secondary antibody (1:500, #A21202, #A21449, #A10042, #A32731, Life Technologies, Carlsbad, California) and Hoechst 33342 (1:1000, #H3570, Invitrogen,) or DAPI (1:1000, #32670, Sigma). After two washes of 3 min with PBSX and one wash of 3 min with DPBS Ca^{2+}/Mg^{2+}, the fixed cells were directly imaged or mounted on microscope slides.

SC slices were fixed in 4% FA for 30 min at RT, washed three times in DPBS and permeabilized (0.7% Triton in PBS) for 10 min at RT. Blocking (Triton 0.5%+FBS 10% in DPBS) was performed for 4 h at 4 °C. Membranes were incubated overnight at 4 °C in primary antibody solution composed by Triton 0.5%, FBS 1% in DPBS and primary antibody: NFL (1:500, #840801, COVANCE, Princeton, New Jersey), Nestin (1:200, #MAB1259, R&D, Minneapolis, Minnesota), cCASP3 (1:200, #AB3623, Millipore). Then, the samples were washed three times in DPBS and incubated in secondary antibody solution (Triton 0.5%, FBS 1% in DPBS and secondary antibody (#A-21244, #A21202, Life Technologies) at working dilution 1:500 for 3 h at RT in dark condition. Slices were washed three times in DPBS for 10 min, mounted on glass slices by using Aqua-Poly/Mount solution (18606-20, Polysciences) and examined using a confocal microscope.

All images were acquired using a fluorescent microscope (TE2000-U, Nikon, Tokyo, Japan) equipped with DS-Ri2 camera or a laser scanning confocal microscope (Eclipse Ti, Nikon). With the fluorescent microscope, images were acquired with a 10× objective and 1024 × 1024 pixel resolution, while 60× and 20× objective oil immersion were used with the laser scanning confocal microscope. Here, series of ≈40 optical plans in Z were acquired at 1024 × 1024 pixel resolution with a z-step of 0.2 µm for cells and 3–6 µm for slices. Images were acquired with a 405 nm laser (425–475 emission filter) or a 488 nm laser (500–550 emission filter) or a 561 laser (570–620 emission filter) or a 640 nm laser (663–738 emission filter) and using an exposure time of 100 ms.

Transmission Electron Microscopy Analysis: NES cells, plated on 8 mm glass coverslips at the density of 1×10^5 cells cm^{-2}, were treated as previously described.[28] Briefly, cells were fixed with 1.5% glutaraldehyde in Na Cacodylate buffer (0.1 M, pH 7.4), washed in the same buffer and postfixed with reduced osmium tetroxide solution (1% K$_3$Fe(CN)$_6$ + 1% OsO$_4$ in Na Cacodylate buffer). After rinses, NES cells were stained with X solution diluted 1:10 v/v in 20% ethanol/water,[68] then dehydrated with a series of ethanol solutions of increasing concentration. Cells were finally embedded in epoxy resin (Epoxy embedding medium kit, Merck KGaA) that was then baked for 24 h at 60 °C. After parting resin from coverslips, samples were sectioned with UC7 ultramicrotome (Leica Microsystems, Wetzlar, Germany) in 80 nm thicker sections and collected on 300 mesh copper grids (G300Cu – Electron Microscopy Science). Grids were finally analyzed with a Zeiss Libra 120 Plus transmission electron microscope, operating at 120 kV and equipped with an in-column omega filter (for the energy filtered imaging) and 16-bit CCD camera 2 k × 2 k bottom mounted (Zeiss, Oberkichen, Germany). 8000× magnification micrographs were collected for the quantitative analysis of cells ultrastructure.

Electrophysiology: SC-NES-derived neurons were recorded by adapting the protocols described in ref. [28,69]. Cultures were continuously perfused with oxygenated Tyrode's solution containing (in mM): NaCl 150, KCl 4, MgCl$_2$ 1, CaCl$_2$ 4, Glucose 10, HEPES 10, pH 7.4 with NaOH. Borosilicate glass pipettes were pulled to a resistance of 4–6 MΩ using a PC-100 puller (Narishige, Japan) and filled with an internal solution containing (in mM): K-Gluconate 145, MgCl2 2, HEPES 10, EGTA 0.1, Mg-ATP 2.5, Na-GTP 0.25, phosphocreatine 5, pH 7.35 with KOH. After achieving a stable whole-cell configuration, the amplifier was switched to current clamp mode and the holding current was adjusted to have an initial membrane potential of −70 mV. Then, a depolarizing step of 20–25 pA was applied and the number of action potentials fired was recorded. The resting membrane potential and spontaneous spiking activity were measured for at least 1 min in $I = 0$ configuration. Data were acquired using a MultiClamp 700A amplifier, connected to a Digidata 1550B digitizer (Molecular Devices, San Jose, California) and analyzed using Clampfit 11.2 (Molecular Devices).

Image Analysis: In short-term stretching assay of in vitro SC-NES cells, the analyses were performed by tracing single neural processes (Figure S1A, Supporting Information). The elongation was measured by using the plugin NeuronJ.[70] 200 non-interconnected TUBB3-stained neural processes (cut-off 20 µm) were analyzed from 10× magnification images (randomly acquired). Ex vivo, hNestin positive processes were traced (Figure S6, Supporting Information) from 10×-magnification images (randomly acquired). For process thickness, a population of 40 crystal violet-stained neural processes was analyzed from randomly acquired 10× magnification images. For each cell, the longest neural process l has been considered and measured. After threshold normalization, binary conversion, the occupied area A related to that neural process has been estimated and the thickness s was calculated as $s = A/l$. For the analysis of in vitro and ex vivo directionality, processes were traced with NeuronJ. The starting and the end points of each tracing were used to calculate the direction of each process. Then, for the in vitro analysis, the angle θ between the direction of each process and the radial direction of the applied force was measured and collected to compare the OIs. For the ex vivo analysis, the angle θ between the direction of each process and the applied force, corresponding to the dorso-ventral axis direction, was measured and collected to compare the OIs. For the analysis of fluorescence, from 60× magnification images (randomly acquired), the integrated density of each cell was measured

with the image analysis software ImageJ, and normalized for the relative area calculated after threshold normalization.

For long-term stretching assay, network analysis methods were chosen. The area of the neural process network was evaluated from 10× magnification images (randomly acquired) obtained from a composition of four 20× images. For each image, the network area was calculated as the ratio of the area occupied by neural processes (after nuclei's area subtraction) and the number of nuclei, automatically counted with the function "analyze particle" of Fiji software. For the analysis of cell dispersion, the center of mass of all nuclei was measured from 10× randomly acquired magnification images obtained from a composition of four 20× images. For each image, the presence of the nuclei was detected thanks to the "Analyze particles" function of ImageJ software, after threshold setting. The center of mass of all nuclei was measured. Subsequently, for each nucleus, the distance between its center of mass and the one of the nearest nucleus was calculated and the dispersion analyzed. In order to provide an evidence of different network morphology, the mean node distance $\overline{d}$ was defined as:

$$\overline{d} = \overline{\min_{i,j=1..n} |N_i - N_j|} \tag{2}$$

with a network of nodes N (center of mass of each cell soma) and arcs d (distance between nodes), being n the total number of nodes.

The fluorescence of the neural process network was evaluated from 60× magnification images randomly acquired. The fluorescence as the integrated density of the neural processes was measured with ImageJ software and normalized for the relative network's area, after nuclei subtraction. The synapse density was estimated by evaluating the number of colocalization spots of pre- and post-synaptic markers, individuated by the plugin puncta analyzer, as previously described.[71] Briefly, both channels were converted using the maximum intensity of the Z projection and merged. Following the identification of a specific ROI corresponding to a process of the cell, and keeping default parameters, the plugin quantifies the puncta in each channel and the co-localized puncta between the two channels. The obtained information was then normalized for the considered area. 63× magnification images were used to perform this analysis. Cellular differentiation was determined by manually counting individual cells labeled for SOX2 or RBFOX3 and expressing them as a percentage of the total number of cells in the field (e.g., positive for DAPI). To perform this analysis, 10× magnification images (randomly acquired) obtained from a composition of four 20× images were used. Similarly, for the evaluation of cell viability and proliferation, cells positive for the markers cCASP3 or pHH3 were manually counted and expressed as a percentage of the total number of cells in the field.

TEM Analysis: TEM analysis was performed using ImageJ and the plugin NeuronJ.[72] Particularly, for the quantification of MNPs, individual MNPs identified as black electro-dense spots were manually counted from cytoplasm of neural processes. The number of MNPs per unit of considered process volume was determined, obtaining one value per process. For the evaluation of ER density, the length of ER cisternae recognized as oblong structures delimited by a single membrane enclosing a single internal space and often associated with ribosomes was traced and measured with NeuronJ, and normalized for the total area of the neural process considered. For microtubule density quantification, the number of microtubules identified as tubular structures was manually counted in cytoplasm of the neural processes. Then, the obtained value was normalized for the diameter of the corresponding region of the neural process, giving one value per neural process. For the cytoskeletal composition the same data were used, comparing the number of neural processes with microtubules and the ones without (e.g., with microfilaments).

Statistical Analysis: Data are reported as mean ± standard deviation (SD) or standard error of the mean (SEM) from at least four separate experiments after blinded analyses (except immunostaining against SOX2/RBFOX3: three separate experiments; TEM data: two separate experiments). Data were plotted with GraphPad software, version 6.0. The normality of the distribution was assayed by different tests, such as D'Agostino & Pearson normality test, Shapiro-Wilk normality test, or KS normality test. For normally distributed data, one-way, two-way analysis of variance (ANOVA) test or t-test for unpaired data followed by Bonferroni correction were used. For non-normally distributed data, Kolmogorov–Smirnov test, Mann–Whitney, or Kruskal–Wallis test analyses were carried out. Significance was set at $p \leq 0.05$.

Supporting Information

Supporting Information is available from the Wiley Online Library or from the author.

Conflict of Interest

The authors declare no conflict of interest.

Data Availability Statement

All metadata, data and data analyses are available at: https://unipiit-my.sharepoint.com/:f:/g/personal/m_baggiani1_studenti_unipi_it/Ejof0ujWo3RPg0j0uWPJCAYBKxby53ZtNzpzPoQsiTsidA?e=tfrmOL. The authors' team adhere to the FAIR criteria on Findability, Accessibility, Interoperability, and Reuse of scientific data.

[1] J. Stiles, T. L. Jernigan, *Neuropsychol. Rev.* **2010**, *20*, 327.

[2] J. C. Silbereis, S. Pochareddy, Y. Zhu, M. Li, N. Sestan, *Neuron* **2016**, *89*, 248.

[3] J. J. Breunig, T. F. Haydar, P. Rakic, *Neuron* **2011**, *70*, 614.

[4] B. Z. Barkho, H. Song, J. B. Aimone, R. D. Smrt, T. Kuwabara, K. Nakashima, F. H. Gage, X. Zhao, *Stem Cells Dev.* **2006**, *15*, 407.

ADVANCED
SCIENCE NEWS

www.advancedsciencenews.com

NANO · MICRO
small
www.small-journal.com

[5] Q. Shen, S. K. Goderie, L. Jin, N. Karanth, Y. Sun, N. Abramova, P. Vincent, K. Pumiglia, S. Temple, *Science* **2004**, *304*, 1338.

[6] S. Temple, *Nature* **2001**, *414*, 112.

[7] D. C. V. Essen, *Nature* **1997**, *385*, 313.

[8] A. Kumar, J. K. Placone, A. J. Engler, *Development* **2017**, *144*, 4261.

[9] H. Abuwarda, M. M. Pathak, *Curr. Opin. Cell Biol.* **2020**, *66*, 104.

[10] K. H. Vining, D. J. Mooney, *Nat. Rev. Mol. Cell Biol.* **2017**, *18*, 728.

[11] L. Luo, D. D. M O'Leary, *Annu. Rev. Neurosci.* **2005**, *28*, 127.

[12] V. Raffa, *Semin. Cell Dev. Biol.* **2023**, *140*, 3.

[13] D. E. Discher, P. Janmey, Y. Wang, *Science* **2005**, *310*, 1139.

[14] S. Chatelin, A. Constantinesco, R. Willinger, *Biorheology* **2010**, *47*, 255.

[15] K. Franze, *Development* **2013**, *140*, 3069.

[16] T. Nishimura, H. Honda, M. Takeichi, *Cell* **2012**, *149*, 1084.

[17] M. Suzuki, H. Morita, N. Ueno, *Dev., Growth Differ.* **2012**, *54*, 266.

[18] A. Fattah, A. Rahman, A. Ranga, *Front Bioeng. Biotechnol.* **2020**, *8*, 240.

[19] S. Rammensee, M. S. Kang, K. Georgiou, S. Kumar, D. V. Schaffer, *Stem Cells* **2017**, *35*, 497.

[20] M. M. Pathak, J. L. Nourse, T. Tran, J. Hwe, J. Arulmoli, D. T. T. Le, E. Bernardis, L. A. Flanagan, F. Tombola, *Proc. Natl. Acad. Sci. USA* **2014**, *111*, 16148.

[21] J. Arulmoli, M. M. Pathak, L. P. McDonnell, J. L. Nourse, F. Tombola, J. C. Earthman, L. A. Flanagan, *Stem. Cells Int.* **2015**, *5*, 8499.

[22] Y.-J. Chang, C.-J. Tsai, F.-G. Tseng, T.-J. Chen, T.-W. Wang, *Biol. Med.* **2013**, *9*, 345.

[23] R. Dai, Y. Hang, Q. Liu, S. Zhang, L. Wang, Y. Pan, H. Chen, *J. Mater. Chem. B* **2019**, *7*, 4161.

[24] A. Kunze, P. Tseng, C. Godzich, C. Murray, A. Caputo, F. E. Schweizer, D. Di Carlo, *ACS Nano* **2015**, *9*, 3664.

[25] W. Pita-Thomas, M. B. Steketee, S. N. Moysidis, K. Thakor, B. Hampton, J. L. Goldberg, *Biol. Med.* **2015**, *11*, 559.

[26] V. Raffa, F. Falcone, S. De Vincentiis, A. Falconieri, M. P. Calatayud, G. F. Goya, A. Cuschieri, *Biophys. J.* **2018**, *115*, 2026.

[27] C. Riggio, M. P. Calatayud, M. Giannaccini, B. Sanz, T. E. Torres, R. Fernández-Pacheco, A. Ripoli, M. R. Ibarra, L. Dente, A. Cuschieri, G. F. Goya, V. Raffa, *Biol. Med.* **2014**, *10*, 4161.

[28] S. De Vincentiis, A. Falconieri, M. Mainardi, V. Cappello, V. Scribano, R. Bizzarri, B. Storti, L. Dente, M. Costa, V. Raffa, *J. Neurosci.* **2020**, *40*, 4997.

[29] B. J. Pfister, A. Iwata, D. F. Meaney, D. H. Smith, *J. Neurosci.* **2004**, *24*, 7978.

[30] A. Falconieri, S. De Vincentiis, V. Cappello, D. Convertino, S. Ghignoli, S. Figoli, S. Luin, F. Català-Castro, L. Marchetti, U. Borello, M. Krieg, V. Raffa, *Cell Rep.* **2023**, *42*, 111912.

[31] M. B. Steketee, S. N. Moysidis, X.-L. Jin, J. E. Weinstein, W. Pita-Thomas, H. B. Raju, S. Iqbal, J. L. Goldberg, *Proc. Natl. Acad. Sci. USA* **2011**, *108*, 19042.

[32] A. Falconieri, N. Taparia, S. De Vincentiis, V. Cappello, N. J. Sniadecki, V. Raffa, *Biophys. J.* **2022**, *121*, 374.

[33] Y. Wang, B. Li, H. Xu, S. Du, T. Liu, J. Ren, J. Zhang, H. Zhang, Y. Liu, L. Lu, *J. Nanobiotechnol.* **2020**, *18*, 64.

[34] M. T. Dell'Anno, X. Wang, M. Onorati, M. Li, F. Talpo, Y. Sekine, S. Ma, F. Liu, W. B. J. Cafferty, N. Sestan, S. M. Strittmatter, *Nat. Commun.* **2018**, *9*, 3419.

[35] M. Onorati, Z. Li, F. Liu, A. M. M. Sousa, N. Nakagawa, M. Li, M. T. Dell'Anno, F. O. Gulden, S. Pochareddy, A. T. N. Tebbenkamp, W. Han, M. Pletikos, T. Gao, Y. Zhu, C. Bichsel, L. Varela, K. Szigeti-Buck, S. Lisgo, Y. Zhang, A. Testen, X. B. Gao, J. Mlakar, M. Popovic, M. Flamand, S. M. Strittmatter, L. K. Kaczmarek, E. S. Anton, T. L. Horvath, B. D. Lindenbach, N. Sestan, *Cell Rep.* **2016**, *16*, 2576.

[36] S. De Vincentiis, A. Falconieri, F. Mickoleit, V. Cappello, D. Schüler, V. Raffa, *Int. J. Mol. Sci.* **2021**, *22*, 4126.

[37] V. Raffa, F. Falcone, M. P. Calatayud, G. F. Goya, A. Cuschieri, *Biophys. J.* **2018**, *115*, 2026.

[38] C. Riggio, M. P. Calatayud, M. Giannaccini, B. Sanz, T. E. Torres, R. Fernández-Pacheco, A. Ripoli, M. R. Ibarra, L. Dente, A. Cuschieri, G. F. Goya, V. Raffa, *Nanomed. Nanotechnol. Biol. Med.* **2014**, *10*, 1549.

[39] J.-A. Abraham, C. Linnartz, G. Dreissen, R. Springer, S. Blaschke, M. A. Rueger, G. R. Fink, B. Hoffmann, R. Merkel, *Langmuir* **2019**, *35*, 7423.

[40] J. I. Valenzuela, F. Perez, *Front. Neurosci.* **2015**, *9*, 358.

[41] D. B. Chklovskii, *Neuron* **2004**, *43*, 609.

[42] A. Pascual-Leone, A. Amedi, F. Fregni, L. B. Merabet, *Annu. Rev. Neurosci.* **2005**, *28*, 377.

[43] M. A. Haendel, K. E. Bollinger, P. W. Baas, *J. Neurocytol.* **1996**, *25*, 289.

[44] M. Khacho, R. Harris, R. S. Slack, *Nat. Rev. Neurosci.* **2018**, *20*, 34.

[45] R. Iwata, P. Vanderhaeghen, *Curr. Opin. Neurobiol.* **2021**, *69*, 231.

[46] S. Mandal, A. G. Lindgren, A. S. Srivastava, A. T. Clark, U. Banerjee, *Stem Cells* **2011**, *29*, 486.

[47] S. Zhang, *World J. Stem Cells* **2014**, *6*, 305.

[48] A. J. Kalyani, D. Piper, T. Mujtaba, M. T. Lucero, M. S. Rao, *J. Neurosci.* **1998**, *18*, 7856.

[49] P. Verstraelen, M. Van Dyck, M. Verschuuren, N. D. Kashikar, R. Nuydens, J. P. Timmermans, W. H. De Vos, *Front Neurosci.* **2018**, *12*, 389.

[50] P. Verstraelen, G.-D. Barriga, M. Verschuuren, B. Asselbergh, R. Nuydens, P. H. Larsen, J.-P. Timmermans, W. H. De Vos, *iScience* **2020**, *23*, 101542.

[51] D. R. Piper, T. Mujtaba, H. Keyoung, N. S. Roy, S. A. Goldman, M. S. Rao, M. T. Lucero, *J. Neurosci. Res.* **2001**, *66*, 356.

[52] O. Hamant, D. Inoue, D. Bouchez, J. Dumais, E. Mjolsness, *Nat. Commun.* **2019**, *10*, 2360.

[53] A. J. Putnam, K. Schultz, D. J. Mooney, *Am. J. Physiol.* **2001**, *280*, C556.

[54] G. G. Farías, A. Fréal, E. Tortosa, R. Stucchi, X. Pan, S. Portegies, L. Will, M. Altelaar, C. C. Hoogenraad, *Neuron* **2019**, *102*, 184.

[55] M. Terasaki, L. B. Chen, K. Fujiwara, *J. Cell Biol.* **1986**, *103*, 1557.

[56] K. Kimura, A. Mamane, T. Sasaki, K. Sato, J. Takagi, R. Niwayama, L. Hufnagel, Y. Shimamoto, J. F. Joanny, S. Uchida, A. Kimura, *Nat. Cell Biol.* **2017**, *19*, 399.

[57] A. Markovinovic, J. Greig, S. M. Martín-Guerrero, S. Salam, S. Paillusson, *J. Cell Sci.* **2022**, *135*, jcs248534.

[58] S. Yogev, R. Cooper, R. Fetter, M. Horowitz, K. Shen, *Neuron* **2016**, *92*, 449.

[59] P. Guedes-Dias, E. L. F. Holzbaur, *Science* **2019**, *366*, eaaw9997.

[60] A. Odawara, H. Katoh, N. Matsuda, I. Suzuki, *Stem Cells Int.* **2016**, *6*, 26181.

[61] K. Togo, H. Fukusumi, T. Shofuda, H. Ohnishi, H. Yamazaki, M. K. Hayashi, N. Kawasaki, N. Takei, T. Nakazawa, Y. Saito, K. Baba, H. Hashimoto, Y. Sekino, T. Shirao, H. Mochizuki, Y. Kanemura, *Mol. Brain.* **2021**, *14*, 149.

[62] E. S. Wilson, K. Newell-Litwa, *Mol. Biol. Cell* **2018**, *29*, 2913.

[63] C. Riggio, S. Nocentini, M. P. Catalayud, G. F. Goya, A. Cuschieri, V. Raffa, J. A. del Río, *Int. J. Mol. Sci.* **2013**, *14*, 10852.

[64] J. Pinkernelle, V. Raffa, M. P. Calatayud, G. F. Goya, C. Riggio, G. Keilhoff, *Front. Neurosci.* **2015**, *9*, 305.

[65] G. Lottini, M. Baggiani, G. Chesi, B. D'Orsi, P. Quaranta, M. Lai, L. Pancrazi, M. Onorati, M. Pistello, G. Freer, M. Costa, *Stem Cell Rep.* **2022**, *17*, 1683.

[66] E. Morelli, E. A. Speranza, E. Pellegrino, G. V. Beznoussenko, F. Carminati, M. Garré, A. A. Mironov, M. Onorati, T. Vaccari, *Front. Cell Dev. Biol.* **2021**, *9*, 637565.

[67] A. Vyas, Z. Li, M. Aspalter, J. Feiner, A. Hoke, C. Zhou, A. O'Daly, M. Abdullah, C. Rohde, T. M. Brushart, *Exp. Neurol.* **2010**, *223*, 112.

[68] A. Moscardini, S. Di Pietro, G. Signore, P. Parlanti, M. Santi, M. Gemmi, V. Cappello, *Sci. Rep.* **2020**, *10*, 11540.

[69] G. Testa, M. Mainardi, E. Vannini, L. Pancrazi, A. Cattaneo, M. Costa, *FASEB J.* **2022**, *36*, e22498.

[70] J. Popko, A. Fernandes, D. Brites, L. M. Lanier, *Cytometry, Part A* **2009**, *75*, 371.

[71] D. M. Ippolito, C. Eroglu, *J. Vis. Exp.* **2010**, *45*, 2270.

[72] E. Meijering, M. Jacob, J.-C. F. Sarria, P. Steiner, H. Hirling, M. Unser, *Cytometry* **2004**, *58A*, 167.